2

ABSORPTION OF MICROWAVES BY ATMOSPHERIC GASES

PHILIP W. ROSENKRANZ

Research Laboratory of Electronics
Massachusetts Institute of Technology
Cambridge, Massachusetts

The transfer of electromagnetic radiation through an atmosphere is linked to its state (temperature, pressure, and composition) by the refractive index and by coefficients for absorption and scattering, if any. The purpose of this chapter is to introduce the physical basis of microwave absorption by atmospheric molecules. A comprehensive exposition of microwave spectroscopy would be beyond the scope of the chapter; instead, O_3, H_2O, CO, N_2O, ClO, O_2, NH_3, N_2 and CO_2 have been chosen as examples, and emphasis is placed on the features of their spectra that have been observed in the terrestrial and planetary atmospheres. (Line parameters are listed in the Appendix to Chapter 2.) However, this group of molecules is sufficiently diverse that some of the discussion here will apply to other molecules of interest. More extensive discussions of molecular spectroscopy can be found in References 1–6.

2.1 GENERAL EXPRESSION FOR ABSORPTION COEFFICIENT

The absorption coefficient in a medium is a macroscopic parameter that represents the interaction of incident electromagnetic energy with the constituent molecules. This interaction is governed by three general principles. First (Bohr's frequency

Atmospheric Remote Sensing by Microwave Radiometry, Edited by Michael A. Janssen
ISBN 0-471-62891-3

condition), the frequency ν of a photon emitted or absorbed by the gas is equal to the difference of two energy levels ($E_a - E_b$) of the gas, divided by Planck's constant h. Second (Einstein's laws of emission and absorption), if E_a is higher than E_b, the probability, given initial state a, of stimulated emission of a photon by a transition from state a to state b is equal to the probability, given initial state b, of absorption of a photon by a transition from b to a. These two probabilities are both proportional to the incident energy at frequency ν. Hence, net absorption (the difference between absorption and stimulated emission) is proportional to the difference in thermodynamic probabilities ($p_b - p_a$) of the two states. Third (Dirac's perturbation theory), for the electromagnetic field to induce transitions between states a and b, the operator with which the field interacts must have a nonzero matrix element linking the two states. For wavelengths that are very long compared to molecular dimensions, this operator is the dipole moment (either electric or magnetic).

In a diffuse isotropic medium, the power absorption coefficient at frequency ν is [7, 8]*

$$\alpha(\nu) = \frac{8\pi^3\nu}{3hcV} \sum_{a,b} \delta(\nu_{ab} - \nu)(p_b - p_a) \sum_{\sigma} |\mathfrak{M}^{\sigma}_{ab}|^2 \tag{2.1}$$

where a and b denote quantum states; $\mathfrak{M}^{\sigma}$ is one of the three spatial components, denoted by the index σ, of the total dipole moment of the molecules within a volume V; $\mathfrak{M}^{\sigma}_{ab}$ is the matrix element of $\mathfrak{M}^{\sigma}$ between a and b; p_a is the thermodynamic probability of state a; $h\nu_{ab} = E_a - E_b$ is the energy difference between states a and b; δ is the Dirac delta function;† and c is the speed of light. The small difference between the propagation speed in a gas and its value in vacuum is not important here.

Equation 2.1 is not in a form useful for actual computation because a and b are states of the entire system of interacting molecules, rather than of isolated molecules. The discussion in this chapter therefore begins in Section 2.2 with the line spectra of isolated molecules. Matrix elements are described at greater length in 2.2.4. The subject of line broadening due to molecular motion and collisions is introduced in Sections 2.3 and 2.4. Finally, Section 2.5 briefly describes absorption due to collision-induced dipole moments.

*Equations, such as Eq. 2.1, that involve a dipole moment assume use of the cgs system. In the SI system, $|\mathfrak{M}^{\sigma}_{ab}|^2$ would be replaced by $|\mathfrak{M}^{\sigma}_{ab}|^2/4\pi\epsilon_0$ for an electric dipole or $\mu_0|\mathfrak{M}^{\sigma}_{ab}|^2$ for a magnetic dipole.

†A molecule in free space has some nonzero probability per unit time of making a spontaneous transition to a lower energy state. This implies, because of Heisenberg's uncertainty principle, that $\delta(\nu_{ab} - \nu)$ should be replaced by a function having unit area but nonzero width. However, this natural line width is negligible for microwave lines, in comparison with the broadening due to other mechanisms to be discussed in this chapter [3, p. 44].

2.2 ENERGY LEVELS AND LINE SPECTRA OF ISOLATED MOLECULES

2.2.1 Born–Oppenheimer Approximation

The motion of the particles—nuclei and electrons—constituting a molecule can be described by a wave function Ψ that depends on the coordinates of all the particles. In the absence of external perturbations, Ψ is expressed as a function of time t by

$$\Psi = \psi e^{-iEt/\hbar} \tag{2.2}$$

where $\hbar$ is $h/2\pi$, and E is the energy of the state represented by a wave function ψ that obeys the time-independent Schrödinger equation [9, p. 53],

$$H\psi = E\psi \tag{2.3}$$

where H is the Hamiltonian operator. Thus, the problem of determining the energy levels of the molecule is one of finding the eigenvalues of the operator H.

Because the electrons in the molecule are very much lighter than the nuclei, and move in fields of roughly the same strength, the electronic motion is more rapid than the motion of the nuclei. In quantum-mechanical terms, the electronic energy levels are generally much more widely spaced than the energies of vibration and rotation of the nuclei. It is possible, therefore, to treat the electronic motion with internuclear distances as parameters, and to treat the motion of the nuclei with the electronic state prespecified. This, the Born–Oppenheimer approximation [9, p. 259], is implemented by separating the wave function into an electronic part and a part for vibration, rotation, and nuclear spin:* $\psi = \psi_{\text{elec}}\psi_{\text{vib-rot-nuc}}$. The eigenvalue problem for electronic motion relative to the nuclei can be solved with a Hamiltonian that includes only electronic kinetic energy and the Coulomb energy of attractions and repulsions among the electrons and nuclei, considering the latter to be fixed. This Hamiltonian, therefore, acts only on ψ_{elec}. The electronic energy, thus calculated as a function of the internuclear distances for each electronic state, then constitutes an effective potential energy for vibrational motion of the nuclei.

In simple molecules such as those that constitute the atmosphere, the vibrational energy levels are generally more widely spaced than the rotational energies, and separation of ψ_{vib} from ψ_{rot} and ψ_{nuc} is appropriate. Then the rotational energy eigenvalue problem can be solved for a prespecified vibrational state, and vice versa. Typically, transitions between electronic states occur in the ultraviolet, vibrational transitions occur in the infrared, and rotational transitions are responsible for microwave, submillimeter, or long infrared lines. Energies associated with interactions involving nuclear spins (hyperfine splitting) are usually equivalent to a few MHz or less.

*For the present, we ignore the translational motion of the molecule, but it will be discussed in Section 2.3.

Pure rotational transitions account for the microwave spectra of H_2O, O_3, CO, and N_2O. The microwave spectra of ClO, O_2 and NH_3 involve some additional interactions, which are discussed in Sections 2.2.10–2.2.12.

2.2.2 Energy Levels and Wave Functions of a Rigid Rotor

Let us consider the rotational Hamiltonian [1, p. 48]:

$$H_{\text{rot}} = \frac{P_x^2}{2I_x} + \frac{P_y^2}{2I_y} + \frac{P_z^2}{2I_z} \tag{2.4}$$

in which I_x, I_y, and I_z are the moments of inertia along the directions of the principal axes of the body (i.e., the principal axes of the ellipsoid of inertia), and P_x, P_y, and P_z are the corresponding components of the angular-momentum operator. The operator representing the square of the total angular momentum has eigenvalues $J(J + 1)\hbar^2$, where J is a nonnegative integer. The component of the angular-momentum operator along a direction fixed in space has eigenvalues $M\hbar$, with M an integer such that $-J \leq M \leq J$ [10, p. 10].

As simple as Eq. 2.4 appears, the solution of Schrödinger's equation with $H = H_{\text{rot}}$ is possible in closed form only for the special case where two of the principal moments of inertia are equal. These solutions are the symmetric-top wave functions. Their importance lies not in being exact wave functions for any particular molecule, but rather because they provide a basis in terms of which the rotational wave functions of any molecule can be expanded. The symmetric-top wave functions are distinguished by the quantum numbers J, M, and a third quantum number K, where $K\hbar$ is the projection of the angular momentum on the axis of symmetry. K must be an integer satisfying $-J \leq K \leq J$. The wave functions are of the form [5, p. 120; 9, p. 275].

$$\psi_{JKM} = \Theta_{JKM}(\theta) e^{iM\phi} e^{iK\chi} \tag{2.5}$$

where the functions Θ_{JKM} are related to the hypergeometric function; θ and ϕ are the polar and azimuthal angles, respectively, which specify the orientation of the axis of symmetry with respect to a set of space-fixed axes; and χ measures the angle of rotation of the top about its axis of symmetry; θ, ϕ, and χ are known as the Euler angles [10, p. 6].

If z is the symmetry axis, then $I_x = I_y$ and H_{rot} can be written as $(P^2 - P_z^2)/2I_x + P_z^2/2I_z$, where P^2 is the square of the total angular momentum. The eigenvalues of H_{rot} for the symmetric top are, therefore,

$$E_{\text{rot}} = h[BJ(J + 1) + (A - B)K^2] \tag{2.6}$$

where

$$A = \frac{h}{8\pi^2 I_z} \tag{2.7a}$$

and

$$B = \frac{h}{8\pi^2 I_x} \tag{2.7b}$$

are rotational constants with dimensions of frequency. In the absence of any interaction (as with a magnetic field) that would establish a preferred direction in space, the energy levels do not depend on M. Furthermore, E_{rot} is unaltered by reversing the sign of K; thus, each energy level with $K \neq 0$ has a degeneracy factor of $2(2J + 1)$, and the $K = 0$ levels are $(2J + 1)$-fold degenerate.

When I_z is smaller than I_x and I_y, the symmetric top is described as prolate; when I_z is larger, it is oblate. The extreme case of a prolate top is a linear molecule, for which the third principal moment of inertia approaches zero. Then A approaches infinity, with the consequence that linear molecules must have $K = 0$. Prolate and oblate symmetric tops share the same set of wave functions, but differ in the coefficient of the K^2 term in Eq. 2.6 and, therefore, in their energy-level structure. For a given J, the general prolate top has energies increasing with $|K|$; for oblate tops, the $|K|$ dependence is reversed.

The planar molecules H_2O and O_3 are asymmetric rotors in the sense of having no two principal moments of inertia equal. The rotational constant $C = h/8\pi^2 I_y$ is defined along with those in Eqs. 2.7a and b, and the axes are conventionally chosen so that $A > B > C$. The degree of asymmetry can be characterized by Ray's parameter,

$$\kappa = \frac{2B - A - C}{A - C} \tag{2.8}$$

which ranges from -1 for prolate symmetry to $+1$ for oblate symmetry. For water, $\kappa = -0.49$; ozone, only slightly asymmetric, has $\kappa = -0.97$.

If one imagines a prolate top being slowly deformed into an oblate top so that κ varies continuously from -1 to 1, the energies of the quantum states also vary in a continuous manner, as illustrated in Fig. 2.1 [11]. However, the projection of angular momentum on the z-axis (or any molecule-fixed axis) is not a constant of the motion for an asymmetric rotor and K, therefore, is no longer a good quantum number. The energy levels nevertheless can be labeled by J and the two values of $|K|$ to which they connect in the limiting cases: these are designated K_{-1} and K_1.*

Figure 2.1 shows the energy levels of different values of J as separated, for the sake of clarity. However, the level spacing depends on the rotational constants of the molecule, and levels with different J's will be interleaved as J increases. This situation gives rise to the rich and complicated rotational spectra of asymmetric molecules.

The rotational wave function for an asymmetric rotor can be expanded in terms

*Another method of labeling the levels is J_τ, where the subscript is an integer, $-J \leq \tau \leq J$, increasing with energy. The two types of subscripts are related by $\tau = K_{-1} - K_1$.

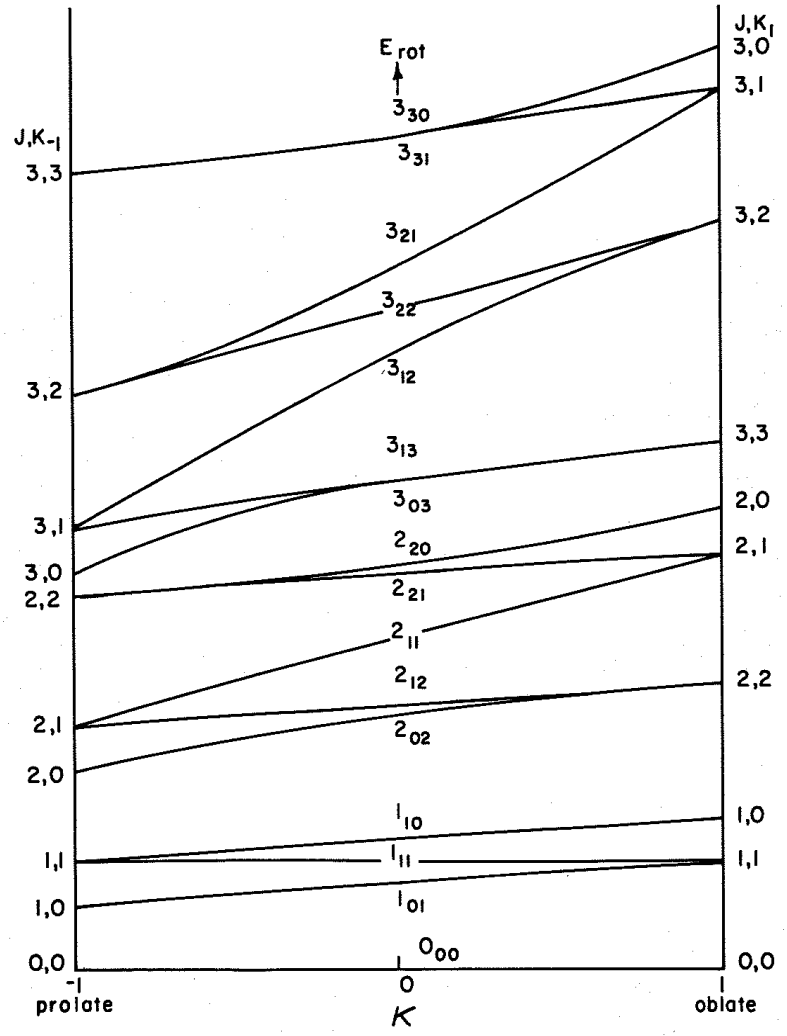

Figure 2.1. The energy levels of a rigid rotor for $J = 0$ to 3, as a function of Ray's asymmetry parameter κ. The vertical spacing of levels depends on the rotational constants.

of symmetric-top wave functions:

$$\psi_{\text{rot}} = \sum_K a_{JK} \psi_{JKM} \tag{2.9}$$

where the coefficients a_{JK} depend on which axis of the molecule is defined to be the z-axis [1, p. 95]. If the axis having the least moment of inertia is chosen, the expansion is termed prolate; if the axis with the greatest moment of inertia is chosen, it is oblate. A rotation by 180° about the z-axis changes ψ_{JKM}, Eq. 2.5, by the factor $\exp(i\pi K) = (-1)^K$; thus, it is symmetric or antisymmetric as K has even or odd parity, respectively.

Even for an asymmetric rotor, the ellipsoid of inertia is invariant under a 180° rotation about any of the three principal axes. The rotational Hamiltonian given

by Eq. 2.4 is specified by the principal moments of inertia, so the effect of this rotation on ψ_{rot} can be only to multiply it by a constant factor c. Two 180° rotations about the same axis are equivalent to no rotation. Thus, $c^2 = 1$ and $c = \pm 1$; that is, ψ_{rot} must be either a symmetric or antisymmetric wave function. Hence, the expansion (Eq. 2.9) will contain terms of only even K or only odd K, and their parity will be the same as K_{-1} if the expansion is prolate, or the same as K_1 if it is oblate. Consequently, ψ_{rot} is multiplied by $(-1)^{K-1}$ for a 180° rotation about the axis of least moment of inertia, and by $(-1)^{K_1}$ for a 180° rotation about the axis of greatest moment of inertia. The symmetry of ψ_{rot} under a 180° rotation about the intermediate axis must then be the same as for a combination of rotations about the other two, because successive 180° rotations about three orthogonal axes return an object to its original position. These symmetry properties are summarized in Table 2.1; they will be used in the discussion of statistical weights and selection rules.

The symmetry properties of linear rotor wave functions can be inferred from Figure 2.1 and Table 2.1 if we recall that a linear molecule is a prolate rotor having $K_{-1} = 0$. Inspection of Figure 2.1 shows that in the $J_{K_{-1}K_1}$ designation system, the linear rotor wave functions are J_{0J}; thus, they are symmetric in a 180° rotation about either the b- or c-axis (i.e., an end-for-end interchange) if J is even, and antisymmetric if J is odd.

This section has described rotating rigid bodies. Real molecules are not rigid, and their moments of inertia depend on their rotational and vibrational states. Accurate calculation of line frequencies generally requires the inclusion of terms in the Hamiltonian to account for centrifugal stretching [12–15]. Vibrational and centrifugal distortion of symmetric-top molecules lowers their symmetry and tends to remove the twofold degeneracy associated with the quantum number $|K|$ for a rigid symmetric top. Section 2.2.12 discusses vibration in connection with the microwave spectrum of NH_3.

TABLE 2.1 Symmetry Properties and Nuclear Spin Degeneracies of Rotational Levels

Parity of		Symmetry of Rotational Wave Function with Respect to 180° Rotation about Axis[a]			Statistical Weight due to Nuclear Spin	
K_{-1}	K_1	a	b	c	$H_2{}^{16}O$	$^{16}O_3$ or $S^{16}O_2$
e[b]	e	1	1	1	1	1
o[b]	o	−1	1	−1	1	1
e	o	1	−1	−1	3	0
o	e	−1	−1	1	3	0

[a]Axis a has the least moment, axis b the intermediate, moment, and axis c the greatest moment of inertia.

[b]e, even; o, odd.

2.2.3 Degeneracies Due to Nuclear Spin

In molecules whose nuclei have nonzero spin, coupling of the spin with the rotational or electronic angular momentum leads to hyperfine splitting of the rotational energy levels. In the approximation that hyperfine splitting is negligible, the resulting degeneracy becomes a factor in the statistical weight of each level, and also in the associated line intensities.

If there are two or more equivalent nuclei (i.e., nuclei of the same isotope and situated in equivalent positions) in a molecule, the quantum statistics of these nuclei produce consequences for its line spectrum. Nuclei of even mass number, and consequently having integer spin, obey Bose–Einstein statistics, which means that the total wave function $\psi = \psi_{\text{elec}}\psi_{\text{vib}}\psi_{\text{rot}}\psi_{\text{nuc}}$ must be symmetric with respect to an operation that interchanges two equivalent nuclei. Nuclei of odd mass number (thus having half-integer spin) obey Fermi–Dirac statistics, which require that ψ be antisymmetric in the same type of operation [9, p. 402]. Rotational wave functions of different symmetries, therefore, must be combined with nuclear-spin wave functions of the appropriate symmetry to make the total wave function either symmetric or antisymmetric, as required. The details of how this occurs depend on the molecule and are therefore deferred to the sections describing individual molecules (e.g., 2.2.6, 2.2.7, 2.2.11, and 2.2.12). However, the result is that rotational states of different symmetry will have unequal statistical weights in molecules with equivalent nuclei.

2.2.4 Selection Rules for Rotational Transitions

If there is no interaction between molecules, the quantum states in Eq. 2.1 become products of states of isolated molecules. The dipole moments of different molecules are then uncorrelated, so

$$|\mathfrak{M}_{ab}^{\sigma}|^2 = nV|\mu_{ab}^{\sigma}|^2 \tag{2.10}$$

where n is the number density of molecules, and $\boldsymbol{\mu}$ is the dipole moment of a single molecule, resulting from the nuclear and electronic charge distributions.

Let us consider the case where a and b denote different rotational states. The orientation of a molecule with respect to a set of space-fixed axes can be specified by the three Euler angles, θ, ϕ, and χ. The component of $\boldsymbol{\mu}$ along any space-fixed axis, for example, μ^Z, is determined by the cosine of an appropriate angle, so it is an operator on the rotational wave functions, and $\boldsymbol{\mu}$ is, therefore, a vector operator. The matrix element of μ^Z linking states a and b can be equated to an integral of the form

$$\mu_{ab}^{Z} = \mu \int\int\int \psi_a^*(\theta, \phi, \chi) \cos\beta\, \psi_b(\theta, \phi, \chi)\, d(\cos\theta)\, d\phi\, d\chi \tag{2.11}$$

where β is the angle between the dipole moment and the space-fixed Z-axis (if the dipole moment is used to define the molecule's z-axis, then $\beta = \theta$), and μ is the magnitude of the dipole moment.

The function cos β is antisymmetric under an operation that reverses the direction of the dipole moment. For example, if $\boldsymbol{\mu}$ is parallel to the b-axis of the molecule, as is the case for H_2O and O_3, then rotation by 180° about either the a- or c-axes is such an operation. However, we have already seen that the rotational wave functions are either symmetric or antisymmetric for a 180° rotation about a principal axis of the molecule. If ψ_a and ψ_b both have the same symmetry, then the integral in Eq. 2.11 will yield zero. The same statement evidently applies to all three components μ_{ab}^{σ} because the definition of the Z-direction in space is arbitrary. In order to have a nonzero matrix element, ψ_a and ψ_b must have opposite symmetry for rotation about either of the two axes perpendicular to the dipole moment, if it is parallel to one of the principal axes. If this is the b-axis, then Table 2.1 shows that the dipole-moment matrix element linking two states will be nonzero only for transitions of the types $ee \leftrightarrow oo$ or $eo \leftrightarrow oe$. Selection rules for dipole moments parallel to the a- or c-axis can be obtained from the table in the same way.

If a 180° rotation about one of the principal axes of a molecule has the sole effect of interchanging two equivalent nuclei, then that axis must contain the electric dipole moment (if the molecule has one). Inspection of Table 2.1 shows that the symmetry properties of any two wave functions are the same with respect to rotation about the axis containing the dipole moment if they are simultaneously opposite with respect to rotations about the other two axes. Hence, the statistical weights due to nuclear spin of the two states in a radiating transition are equal. This statement is true in general of molecules containing equivalent nuclei [5, p. 138; 6, p. 55].

The θ variation of a symmetric-top wave function, where θ is the angle between the molecule's z-axis and the space-fixed Z-axis, is given by a function $\Theta_{JKM}(\theta)$. The orthogonality properties of these functions, when combined in integrals such as Eq. 2.11, are such that any dipole-moment matrix element can be nonzero only if $|J_a - J_b| \leq 1 \leq J_a + J_b$ [3, p. 29], where J_a and J_b are the quantum numbers for total angular momentum of the two states. Because asymmetric rotor wave functions can be expressed by Eq. 2.9, where the sum involves ψ_{JKM} all with the same J, this selection rule applies to rotational wave functions for all molecular shapes.

2.2.5 Line Intensities

For computational purposes, it is generally useful to rewrite Eq. 2.1 in the form

$$\alpha(\nu) = n \sum_{f,i} S_{fi}(T) F(\nu, \nu_{fi}) \tag{2.12}$$

where $\alpha(\nu)$ is the power-absorption coefficient due to a specified molecular species, n is the number of molecules of this species per unit volume, f and i denote energy levels of an isolated molecule, $S_{fi}(T)$ is the intensity at temperature T of a single line for a single molecule, and $F(\nu, \nu_{fi})$ is a line-shape function normalized in such a way that $F(\nu, \nu_{fi}) \rightarrow \delta(\nu - \nu_{fi})$ for isolated molecules. (Line shapes are

discussed in Sections 2.3 and 2.4.) As written, the summation in Eq. 2.12 extends over all combinations of f and i, thus including line frequencies $\nu_{fi} = (E_f - E_i)/h$ that are negative as well as positive; but more often, one would restrict the summation to positive line frequencies and include the negative-resonant term in $F(\nu, \nu_{fi})$ (if necessary, in the pressure range of interest). The summation then need include only those lines that contribute to the frequency range of interest.

Making use of the ideal gas law, one has

$$n = \frac{aP}{kT} \tag{2.13}$$

where P is the partial pressure of the absorbing gas, and a is the fractional abundance of the specified isotopic variant of the molecule. Isotopic substitutions in a molecule alter the transition frequencies because of the different masses of the nuclei. When more than one absorbing species is present, the total absorption coefficient is given by the sum of absorption coefficients for each species.

The line intensity consistent with Eqs. 2.1, 2.10, and 2.12 is

$$\begin{aligned} S_{fi}(T) &= \frac{8\pi^3 \nu_{fi} (\mu_{fi})^2 \, g_i}{3hcQ(T)} \left(e^{-E_i/kT} - e^{-E_f/kT} \right) \\ &= \frac{16\pi^3 \nu_{fi} (\mu_{fi})^2 \, g_i}{3hcQ(T)} \sinh (h\nu_{fi}/2kT) e^{-(E_f + E_i)/2kT} \end{aligned} \tag{2.14}$$

in which a Maxwell–Boltzmann distribution of state occupation probabilities (implying local thermodynamic equilibrium) has been used; g_i is the statistical weight due to nuclear spin for level i,

$$Q(T) = \sum_i g_i (2J_i + 1) e^{-E_i/kT} \tag{2.15}$$

is the internal partition function; and μ_{fi} is the reduced (meaning that it does not depend on the orientational quantum numbers M) matrix element, between levels f and i, of the molecular dipole moment, measured in esu-cm for an electric dipole or erg/gauss for a magnetic dipole. $(\mu_{fi})^2$ is equal to the sum of the squared magnitudes of matrix elements over the degenerate orientational states of levels f and i and also over the three spatial components σ [10, p. 76]. We note that $|\mu_{fi}| = |\mu_{if}|$ and $g_i = g_f$ (see Section 2.2.4).

When ν_{fi} (GHz) $< 10T$ (Kelvin), Eq. 2.14 is approximated within 1% by

$$S_{fi}(T) = \frac{8\pi^3 \nu_{fi}^2 (\mu_{fi})^2 g_i}{3ckTQ(T)} e^{-(E_f + E_i)/2kT} \tag{2.16}$$

If one has a table (as in the Appendix to Chapter 2) of line intensities at a specified temperature T_0 along with the associated energy levels, then $S_{fi}(T)$ can be com-

puted as

$$S_{fi}(T) = S_{fi}(T_0)\frac{T_0 Q(T_0)}{TQ(T)}\exp\left[\frac{E_f + E_i}{2kT_0}\left(1 - \frac{T_0}{T}\right)\right] \tag{2.17}$$

provided that one knows the temperature dependence of Q. Generally, $Q(T)$ can be separated as [6, p. 503]

$$Q(T) = Q_{\text{elec}}(T)Q_{\text{vib}}(T)Q_{\text{rot}}(T) \tag{2.18}$$

For asymmetric (H_2O, O_3) or symmetric-top molecules (NH_3), a good approximation to the temperature dependence of Q_{rot} is [6, p. 505]

$$Q_{\text{rot}}(T)/Q_{\text{rot}}(T_0) = (T/T_0)^{3/2} \tag{2.19}$$

Linear molecules (O_2, N_2O, CO, ClO) have fewer rotational states, and in this case [6, p. 505],

$$Q_{\text{rot}}(T)/Q_{\text{rot}}(T_0) = T/T_0 \tag{2.20}$$

For most molecules, the excited electronic states lie so high in energy that Q_{elec} is very nearly unity. The only exception among the molecules treated here is ClO, for which

$$Q_{\text{elec}}(T) = 1 + \exp(-E_e/kT) \tag{2.21}$$

with $E_e/k = 458$ K [16].

Using a harmonic oscillator model [6, p. 503],

$$Q_{\text{vib}}(T) = \prod_v [1 - \exp(-\hbar\omega_v/kT)]^{-d_v} \tag{2.22}$$

where ω_v is the fundamental frequency of the vth mode of vibration (e.g., a diatomic molecule has one mode of vibration), and d_v is usually 1 but may be 2 if a vibrational mode is degenerate, as is the bending mode of N_2O. (Temperature equivalents of the vibrational frequencies are listed in footnotes to the line tables in the Appendix to this chapter.) In O_2, CO, ClO, H_2O, and NH_3, Q_{vib} can be well approximated by unity at temperatures encountered in the terrestrial atmosphere. In O_3 and N_2O, only the lowest-energy mode of vibration, the bending mode, need be included in Eq. 2.22 at temperatures up to ~300 K.

2.2.6 Rotational Spectrum of Ozone

The three nuclei in $^{16}O_3$ form an angle of 117°. The two outer nuclei are in equivalent positions. These nuclei obey Bose–Einstein statistics, so the total wave func-

tion must be symmetric with respect to an operation that interchanges the outer nuclei. This operation can be represented as the product of two rotations. The first is a rotation of the entire molecule by 180° about the axis passing through the central nucleus and equidistant from the two outer nuclei, in the plane of the molecule. (This axis is the one having an intermediate moment of inertia.) The second rotation, of the electrons with respect to the nuclei, returns the electrons to their original positions. ψ_{elec} is a function of the coordinates of the electrons relative to the nuclei, so it is uninfluenced by the first rotation. The ground state ψ_{elec} is symmetric with respect to the second rotation. ψ_{vib} is a function of the relative coordinates of the nuclei and, therefore, is unchanged by either rotation. The ^{16}O nuclei have zero spin, so there is only one possible ψ_{nuc}, and it is symmetric. Thus, ψ_{rot} must also be symmetric with respect to rotation by 180° about the b-axis. Table 2.1 shows that this condition is satisfied only in states where K_{-1} and K_1 have the same parity; these are the *only* possible rotational states for the ground electronic state of $^{16}O_3$. Numerous microwave transitions occur between these states.

We note in passing that the foregoing statements also apply to $S^{16}O_2$, in which sulfur is substituted for the central atom.

2.2.7 Rotational Spectrum of Water Vapor

In H_2O, the oxygen nucleus lies at the vertex of a 105° angle formed with the hydrogen nuclei, which thus are in equivalent positions. Protons obey Fermi–Dirac statistics, so the total wave function ψ must be antisymmetric with respect to the interchange of the hydrogen nuclei. As in the previous section, this operation involves a 180° rotation about the axis with intermediate moment of inertia. The ground-state electronic wave function is symmetric, so the antisymmetry of ψ depends on ψ_{rot} and ψ_{nuc}.

Let us consider the symmetry properties of ψ_{nuc} for $H_2{}^{16}O$. The ^{16}O nucleus has zero spin. Each hydrogen nucleus has spin quantum number $= \frac{1}{2}$, and the component of the spin operator along an axis fixed in space has eigenvalue $\pm\frac{1}{2}\hbar$. The wave functions associated with these two eigenvalues will be denoted by $\sigma^{\uparrow}$ and $\sigma^{\downarrow}$, and the nucleus to which the wave function pertains will be indicated by a subscript 1 or 2. The space of possible wave functions for ψ_{nuc} thus has four dimensions. The subspace of symmetric spin wave functions is three-dimensional and is spanned by the three wave functions

$$\psi_{\text{nuc}} = \begin{cases} \sigma_1^{\uparrow}\sigma_2^{\uparrow} & \text{(2.23a)} \\ \sigma_1^{\downarrow}\sigma_2^{\downarrow} \text{ or} & \text{(2.23b)} \\ 2^{-1/2}(\sigma_1^{\uparrow}\sigma_2^{\downarrow} + \sigma_1^{\downarrow}\sigma_2^{\uparrow}) & \text{(2.23c)} \end{cases}$$

The subspace of antisymmetric spin wave functions is one-dimensional, with

$$\psi_{\text{nuc}} = 2^{-1/2}(\sigma_1^{\uparrow}\sigma_2^{\downarrow} - \sigma_1^{\downarrow}\sigma_2^{\uparrow}) \qquad \text{(2.24)}$$

To obtain a total wave function ψ that is antisymmetric with respect to the interchange of the hydrogen nuclei, the symmetric ψ_{nuc} (Eq. 2.23) must combine with the ψ_{rot} that are antisymmetric about the axis with an intermediate moment of inertia (b-axis); as shown in Table 2.1, these are the rotational states for which K_{-1} and K_1 are of opposite parity. The antisymmetric ψ_{nuc} (Eq. 2.24) combines with the rotational states that are symmetric about the b-axis: K_{-1} and K_1 having the same parity.

Because of the small moments of inertia of water vapor, most of its strong rotational transitions lie at submillimeter and infrared wavelengths. The two important microwave transitions are at 22.235 and 183.310 GHz. The first of these occurs between nuclear spin triplets of the type (Eq. 2.23) and its splitting is approximately 400 kHz [16a]; the second is between singlet spin states of the type (Eq. 2.24).

Water vapor also has a continuum absorption, which will be described in Section 2.4.3.

2.2.8 Rotational Spectrum of Carbon Monoxide

Carbon monoxide (CO) is a linear molecule, so its rotational energy levels are specified by the first term on the right side of Eq. 2.6. The frequency of a transition from J to $J + 1$ is $2B(J + 1)$, which produces a spectrum of lines at integer multiples of 115.3 GHz.

2.2.9 Rotational Spectrum of Nitrous Oxide

Nitrous oxide has the linear structure N-N-O. The two nitrogen nuclei are not in equivalent positions, so rotation of the molecule does not interchange them. Hence, all rotational levels have the same statistical weight due to nuclear spin.

Rotational transitions lie at integer multiples of $2B = 25.1$ GHz, in the ground vibrational state. In excited vibrational states, interaction between vibrational and rotational motion produces a splitting of levels that is called l-type doubling [3, p. 128]; however, the weaker microwave lines associated with excited states have not yet been observed in the atmosphere.

2.2.10 Rotational Spectrum of Chlorine Monoxide

The electronic state of lowest energy for most molecules is one in which the electrons are paired (the two electrons of a pair have the same quantum numbers except for opposite spins) and in which their orbital angular momenta sum to zero. However, the ClO radical possesses an odd number of electrons and thus has a net electronic-spin angular momentum with quantum number of $\frac{1}{2}$. Furthermore, the ground electronic state is one with orbital angular momentum. In a diatomic molecule, the electrons move in an axially symmetric potential, so they encounter no torque about the internuclear axis. The projection of the orbital angular momentum on that axis is, therefore, a constant of their motion and is characterized by a

quantum number Λ. In the ground state of ClO, $\Lambda = 1$. The electronic orbital angular momentum perpendicular to the axis is not constant.

The electronic spin and orbital motion, and the rotation of the molecule as a whole, generate magnetic fields. Interactions between these fields couple the various angular momenta and separate the energies of states that would otherwise be degenerate. Hund classified the possible types of coupling into five cases, according to the predominant interactions [1, p. 177]. The wave functions and associated quantum numbers apply to a given molecule to the extent that it approximates one of these pure cases.

In ClO, the strongest coupling is that of the electronic spin to the orbital angular momentum along the internuclear axis. This is Hund's case (a). The component of electronic spin along the axis has the possible values $\pm\frac{1}{2}\hbar$. The sum of orbital and spin angular momenta along the axis is given the quantum number Ω. The ground state has $\Omega = \frac{3}{2}$; the $\Omega = \frac{1}{2}$ state is slightly higher in energy and, therefore, is included in the electronic partition function, Eq. 2.21.

The electronic angular momentum then adds vectorially to the rotational angular momentum of the molecule, forming a resultant with quantum number J. The relation between this resultant angular momentum and its projection $\Omega\hbar$ on the internuclear axis is the same as in a symmetric top, so an expression of the form given by Eq. 2.6, with Ω replacing K, is valid for the associated rotational energy. However, Ω is constant in a given electronic state, so it is more appropriate to regard the second term of this expression as part of the electronic energy and to write

$$E_{\text{rot}} = hBJ(J + 1) \tag{2.25}$$

as usual for a linear molecule. Because J cannot be smaller than its projection on the internuclear axis, it has the possible values $\frac{3}{2}, \frac{5}{2}, \frac{7}{2}, \ldots$, in the ground state of ClO. Transitions between levels J and $J + 1$ then give rise to lines at frequencies

$$\nu_{J+1,J} = 2B(J + 1) \tag{2.26}$$

which are spaced at intervals of $2B = 37.2$ GHz [13].

The preceding discussion gives an approximate description of the rotational spectrum of ClO. A more precise description must include the interaction between the magnetic moment associated with the spin of the chlorine nucleus and the magnetic fields generated by the electrons [13]. The nuclear electric quadrupole moment also interacts with the electric-field gradient at the nucleus [13]. These weaker interactions cause the hyperfine splitting of energy levels, which in ClO is $\lesssim 100$ MHz. The levels are distinguished by different values of the total angular momentum, which is the resultant of J and the chlorine nuclear spin. This total angular momentum has quantum number F, with $J - \frac{3}{2} \leq F \leq J + \frac{3}{2}$. (Both ^{35}Cl and ^{37}Cl have nuclear spin of $\frac{3}{2}$.) Hence, for each value of J, there are four levels, each with a different F value. Transitions between different levels have the usual

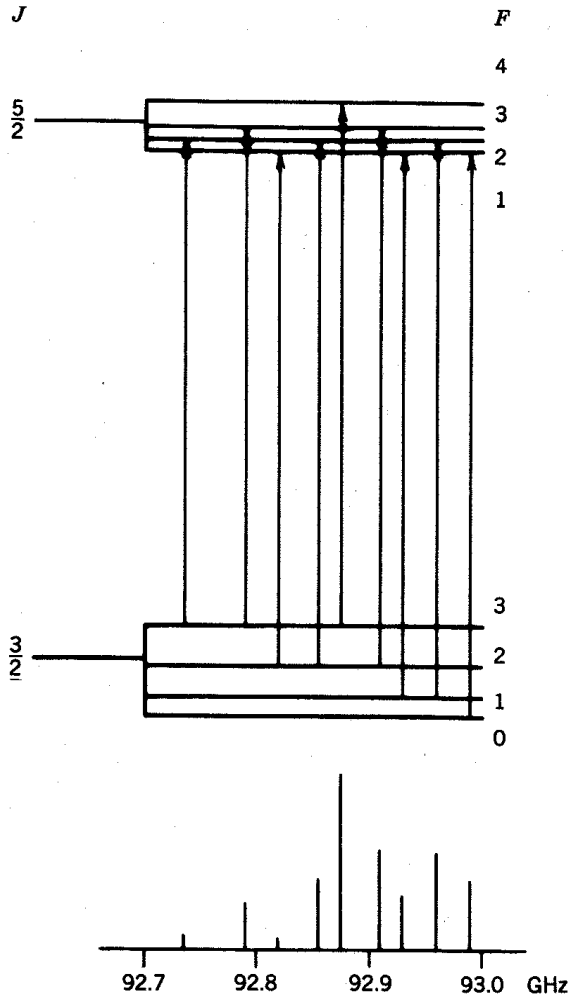

Figure 2.2. Energy-level diagram and hyperfine structure of the $J = \frac{3}{2}$ to $J = \frac{5}{2}$ rotational transition in the ground state of $^{35}Cl^{16}O$ [14].

dipole-moment selection rules: $\Delta F = 0, \pm 1$. Thus, each of the lines corresponding to Eq. 2.26 is split into nine components, as shown in Figure 2.2 for the $J = \frac{3}{2}$ and $\frac{5}{2}$ levels.

Although the component of electronic orbital angular momentum perpendicular to the internuclear axis is not constant, its magnetic interaction with the rotational angular momentum causes a further splitting of the energy levels known as Λ-type doubling [5, p. 226]. In the ground state of ClO, this splitting is $\lesssim 1$ MHz [17]. The electronic angular momentum will interact with an external magnetic field, producing Zeeman splitting [18]. In the Earth's magnetic field, this effect is ~ 1 MHz for the $J = \frac{3}{2}$ to $\frac{5}{2}$ transitions, and it decreases with increasing J. These line splittings do not appear to be significant in the context of observations of ClO in the terrestrial atmosphere.

2.2.11 Spin-Rotation Spectrum of Oxygen

The ground electronic state of O_2 is one in which the orbital angular momentum averages to zero, but there are two unpaired electron spins [19]. The magnetic fields associated with the electron spins interact with each other and with the magnetic field generated by rotation of the molecule. The total spin angular momentum, with a quantum number of 1, adds vectorially to the rotational angular momentum, which is given the quantum number N, to form a resultant angular momentum with quantum number J, where $J = N - 1$, N, or $N + 1$. This is Hund's coupling case (b) [1, p. 178].* The energies of the states with $J = N$ are given in the rigid rotor approximation by

$$E_{J=N} = hBN(N + 1) \tag{2.27}$$

with $B = 43.1$ GHz [15]. The states with $J = N - 1$ and $J = N + 1$ are lower in energy by amounts that, with one exception (at 118.75 GHz), are on the order of $h \cdot 60$ GHz. Because the coupling between spin and rotational angular momentum is rather weak, both N and J are needed to specify an energy level. For example, the state with $J = 2$, $N = 1$ differs in energy from the state with $J = 2$, $N = 3$ by $h \cdot 425$ GHz.

The ground-state electronic wave function of $^{16}O_2$ is antisymmetric with respect to the interchange of the nuclei. This antisymmetry is not affected by the electron-spin orientation in a Hund's case (b) molecule [5, p. 238]. The nuclear spin is zero, and thus the Bose–Einstein requirement for symmetry of the total wave function is met only by antisymmetric rotational wave functions, which are those with *odd* values of the rotational quantum number N (see Section 2.2.2).

The magnetic moment associated with each of the unpaired electrons has a magnitude slightly greater than one Bohr magneton μ_B and is antiparallel to the spin. The total magnetic moment $\boldsymbol{\mu}$ of O_2 (which is essentially due to the electron spins) will interact with an external magnetic field $\mathfrak{H}$ and split the energies of states with different values of the quantum number M, which would otherwise be degenerate. This is the Zeeman effect. The term of the Hamiltonian corresponding to this interaction is [1, p. 284; 21]

$$H_{\text{mag}} = -\boldsymbol{\mu} \cdot \mathfrak{H} = 2.00232\mu_B \boldsymbol{S} \cdot \mathfrak{H} \tag{2.28}$$

where $\boldsymbol{S}$ is the spin operator measured in units of h. We shall consider the case in which $\mathfrak{H}$ is less than a few hundred gauss, so that H_{mag} represents a small perturbation of the Hamiltonian. Then a good approximation to the energy levels can be obtained by adding the diagonal matrix elements of H_{mag} to the energy levels of the Hamiltonian without magnetic field. A diagonal element of H_{mag} is equivalent to the time average of the interaction energy (which is proportional to the electron spin) in one of the states described by a Hund's case (b) wave function. The cou-

*The eigenfunctions for oxygen differ slightly from the ideal case (b), with a resulting modification in the microwave line strengths of $\leq 2\%$ [20].

pling between spin and rotational angular momentum in Hund's case (b) forces the spin vector to precess about the total angular-momentum vector, which then precesses much more slowly about the external magnetic field. The interaction energy Eq. 2.28 is therefore obtained by first projecting the spin onto the total angular momentum and then taking the component of this projection along the external magnetic field [1, p. 286]. Figure 2.3 shows the energy levels for the states with $N = 3$ and $J = 3, 4$. When $J = N$, the rotational angular momentum, the spin, and their resultant form an isosceles triangle, so that the projection of the spin on the total angular momentum is smaller than for the states with $J = N \pm 1$, though not zero.

Oxygen has no permanent electric dipole moment, but it will interact with an electromagnetic wave by means of its magnetic dipole. This interaction is much weaker than that of a typical molecular electric dipole, but the great abundance of oxygen in the atmosphere compensates for the intrinsic weakness of its absorption. Selection rules for magnetic-dipole matrix elements differ in one respect from those for electric dipoles, which were described in Section 2.2.4. Because of its association with angular momentum, a magnetic-dipole moment is an even operator, in contrast to an electric-dipole moment, which is fixed in the molecule and is therefore an odd operator [22]. The magnetic-dipole moment has a nonzero matrix element only between two oxygen wave functions that are both symmetric or both antisymmetric.

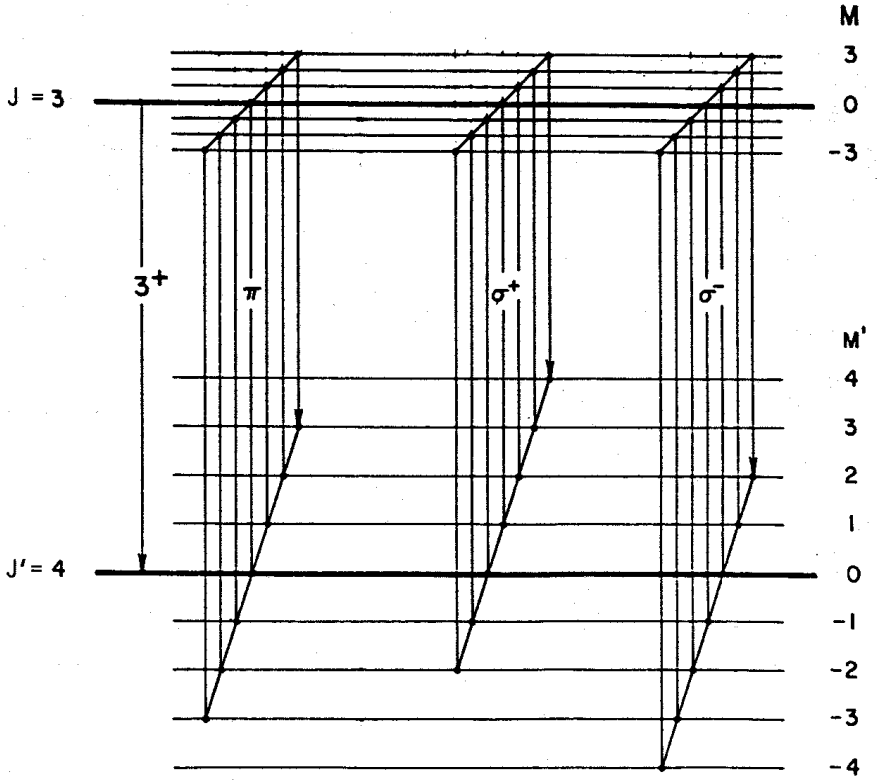

Figure 2.3. Energy-level diagram for the $N = 3$, $J = 3, 4$ states of O_2 [23].

The selection rules with respect to angular momentum quantum numbers are

$$|\Delta J| \leq 1 \leq J + J' \tag{2.29a}$$

and

$$|\Delta M| \leq 1 \tag{2.29b}$$

(The latter rule is of observational consequence only in the Zeeman effect.) These selection rules permit transitions between the levels $J = N$ and $J = N + 1$ (which, conventionally, are designated as $N+$ lines), between $J = N$ and $J = N - 1$ (designated $N-$), or within a given (J, N) level (except the $J = 0$, $N = 1$ level). Transitions between levels $J = N - 1$ and $J = N + 1$ are prohibited. Transitions between levels with different N and $|\Delta J| \leq 1$ are possible, but these produce lines at submillimeter wavelengths [20, 23].

Transitions with $\Delta J = \pm 1$ for which $\Delta M = 0$ are known as π components and those for which $\Delta M = \pm 1$ are $\sigma^{\pm}$ components. Table 2.2 gives the frequency displacements, with respect to the unsplit resonant frequency, for the possible Zeeman components as a function of N and M, the quantum numbers for the upper ($J = N$) levels of the oxygen lines. The limits on possible values of M are set by the smaller of the two values of J involved in a transition; hence, the different limits for $N-$ lines. Table 2.3 gives the intensities of each component, referenced to the unsplit oxygen line intensities listed in Appendix 2A. Figure 2.4 shows the spectrum of Zeeman components for the 3+ line in a field of 0.5 gauss (typical for midlatitudes). Lines with higher N have more components, but they are more closely spaced, giving approximately the same maximum splitting.

If the observation frequency is displaced from a line center by more than ~6 MHz, or if the entire propagation path lies at pressures of more than a few millibars, the Zeeman splitting of an oxygen line can safely be ignored in a radiative transfer calculation for the terrestrial atmosphere. If the observation includes the core of a line formed at low pressures, however, it is necessary to consider the Zeeman effect. In this case, absorption and emission depend on the angle between

TABLE 2.2 Frequency Shifts of O_2 Zeeman Components from Line Center [23][a]

ΔM	$N+$ lines	$N-$ lines
0	$-a\mathcal{H}\dfrac{M(N-1)}{N(N+1)}$, for $\lvert M\rvert \leq N$	$a\mathcal{H}\dfrac{M(N+2)}{N(N+1)}$, for $\lvert M\rvert \leq N-1$
± 1	$-a\mathcal{H}\dfrac{M(N-1)\pm N}{N(N+1)}$, for $\lvert M\rvert \leq N$	$a\mathcal{H}\dfrac{M(N+2)\pm(N+1)}{N(N+1)}$, for $\lvert M\pm 1\rvert \leq N-1$

[a] $a = 2.8026$ MHz/gauss. $\mathcal{H}$ = external magnetic field strength. M = orientational quantum number for the $J = N$ level.

TABLE 2.3 Intensities of O_2 Zeeman Components, Relative to Unsplit Lines [23]

ΔM	$N+$ lines	$N-$ lines
0	$\dfrac{3[(N+1)^2 - M^2]}{(N+1)(2N+1)(2N+3)}$	$\dfrac{3(N^2 - M^2)}{N(2N-1)(2N+1)}$
± 1	$\dfrac{3(N \pm M + 1)(N \pm M + 2)}{4(N+1)(2N+1)(2N+3)}$	$\dfrac{3(N \mp M)(N \mp M - 1)}{4N(2N-1)(2N+1)}$

the terrestrial magnetic field and the direction of propagation of the electromagnetic wave, and on its polarization [24, 24a]. Furthermore, different polarizations in general will be partially coherent, so the coherency-matrix formulation of the radiative transfer equation should be used to calculate brightness temperatures [24, 24a, 25].

However, there are two special cases in which the scalar form of the radiative transfer equation, described in Chapter 1, can be used for Zeeman-split lines. These cases occur when the coherency matrix is diagonal in a fixed polarization basis. If the direction of propagation is perpendicular to the constant magnetic field $\mathfrak{H}$, the characteristic polarizations (which diagonalize the coherency matrix) are linear and either parallel or perpendicular to $\mathfrak{H}$. For the electric field ε_{RF} perpendicular, the microwave magnetic field $\mathfrak{H}_{RF}$ is parallel or antiparallel to $\mathfrak{H}$ and it therefore interacts with the Z-component of the oxygen magnetic moment, where the Z-direction is defined by $\mathfrak{H}$. There is no dependence of this interaction on the azimuthal angle ϕ. The dependence of the rotational wave functions on azimuth is given by a factor of the form $\exp(iM\phi)$, so the matrix element between two rotational states (as in Eq. 2.11) can be nonzero only if $\Delta M = 0$. Thus, the absorption for each line is contributed solely by the π components (dependence on N is omitted for clarity):

$$\alpha(\mathfrak{H}_{RF} // \mathfrak{H}) = n \sum_M S_{M,M}(T) F(\nu, \nu_{M,M}) \tag{2.30}$$

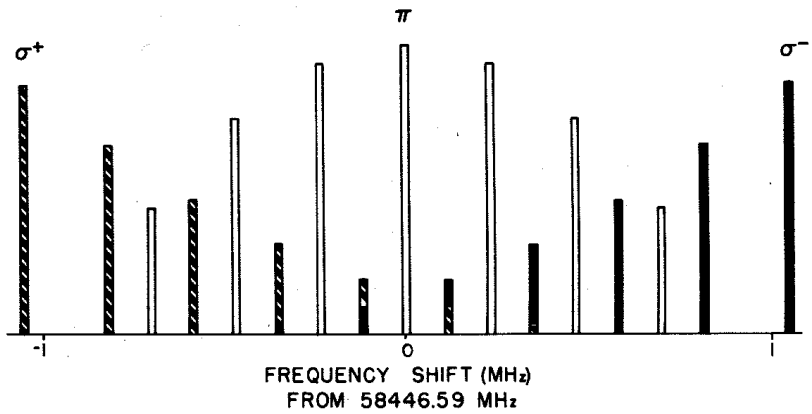

Figure 2.4. Zeeman components of the 3+ oxygen line.

The line-shape function F is discussed in Sections 2.3 and 2.4. For the orthogonal polarization, the interaction between $\boldsymbol{\mu}$ and $\mathcal{H}_{RF}$ has a cos ϕ dependence, and it therefore excites only the σ components:

$$\alpha(\varepsilon_{RF}//\mathcal{H}) = n \sum_M [S_{M,M+1}(T)F(\nu, \nu_{M,M+1}) + S_{M,M-1}(T)F(\nu, \nu_{M,M-1})]. \tag{2.31}$$

The second special case occurs when the direction of propagation is along the magnetic field $\mathcal{H}$. The characteristic polarizations are then right-circular and left-circular. A right-circular wave is absorbed by the σ^+ components:

$$\alpha_{RC} = 2n \sum_M S_{M,M+1}(T)F(\nu, \nu_{M,M+1}) \tag{2.32}$$

and a left-circular wave by the σ^- components:

$$\alpha_{LC} = 2n \sum_M S_{M,M-1}(T)F(\nu, \nu_{M,M-1}) \tag{2.33}$$

If the direction of propagation is antiparallel to $\mathcal{H}$, σ^+ and σ^- are interchanged in Eqs. 2.32 and 2.33.

We note that the intensities of the Zeeman components are defined such that

$$\sum_M S_{M,M}(T) = 2 \sum_M S_{M,M+1}(T) = 2 \sum_M S_{M,M-1}(T) = S(T) \tag{2.34}$$

where $S(T)$ is the intensity of the unsplit line. Thus, the absorption by oxygen becomes unpolarized and isotropic when the observation frequency is displaced from the line center by an amount large compared to the Zeeman splitting.

In the Earth's magnetic field, the resonant frequencies of the $\Delta J = 0$ transitions are $\lesssim 1$ MHz (0 MHz for $\Delta M = 0$). Considering that the line intensity, Eq. 2.16, contains the factor ν_{fi}^2, one might suppose these transitions to be entirely negligible. This would be the case were it not for the effect of collisions between molecules. Equation 2.1 shows that the relevant energy difference is really between two states of the system of interacting molecules. At pressures near 1 atmosphere, the $\Delta J = 0$ matrix elements of oxygen produce a detectable, unpolarized absorption in the GHz range of frequencies. This nonresonant absorption will be discussed further in Section 2.4.

2.2.12 Inversion Spectrum of Ammonia

Ammonia (NH_3) has a tetrahedral structure, with the potential function shown in Figure 2.5 for motion of the nitrogen nucleus perpendicular to the plane of the hydrogen nuclei. The first two wave functions for this mode of motion are also shown. The height of the central barrier in the potential exceeds the kinetic energy

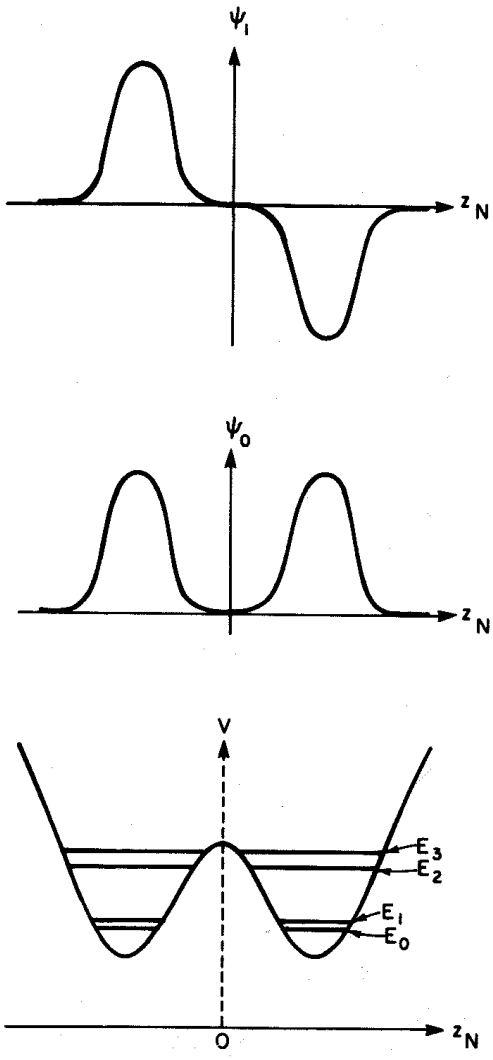

Figure 2.5. Potential-energy function and two lowest-energy wave functions for the position of the nitrogen nucleus relative to the plane of the hydrogen nuclei in NH_3.

associated with each of these two wave functions by more than a factor of 2. Nevertheless, the wave functions have nonzero values inside the barrier; this is an example of the quantum-mechanical tunneling effect. The shape of the potential function depends somewhat on the rotational quantum numbers of the molecule, and the difference in energy between $\psi_0(z_N)$ and $\psi_1(z_N)$ varies inversely with the height of the potential barrier [1, p. 302]. The strongest of the transitions between $\psi_0(z_N)$ and $\psi_1(z_N)$ lies in the 20–30-GHz range [26]. Strictly speaking, these are vibrational transitions, although they often are not classified as such. They are called inversion lines, because the passing of the nitrogen nucleus through the plane of the hydrogens turns the molecule inside out. Transition frequencies for other vibrational modes and for $\psi_1(z_N)$ to $\psi_2(z_N)$ lie in the infrared. Pure rotational transitions of NH_3 produce submillimeter-wavelength lines [27].

The statistical weights of NH_3 rotational levels due to nuclear spin can be deduced from consideration of a rotation by 120° about the axis of symmetry. This

rotation is equivalent to two interchanges of hydrogen nuclei.* Therefore, the total wave function must be symmetric with respect to this operation. In the ground state, ψ_{elec} is symmetric (i.e., with respect to the inverse rotation of the electrons, which returns them to their original position) and ψ_{vib} is unaffected. ψ_{JKM} changes by the factor $\exp(i2\pi K/3)$, which makes it symmetric if K is divisible by 3. If K is not a multiple of 3, we can construct the nuclear spin wave functions

$$\psi_{\text{nuc}}^{K} = \begin{cases} 3^{-1/2}(\sigma_1^{\downarrow}\sigma_2^{\uparrow}\sigma_3^{\uparrow} + e^{i2\pi K/3}\sigma_1^{\uparrow}\sigma_2^{\downarrow}\sigma_3^{\uparrow} + e^{i4\pi K/3}\sigma_1^{\uparrow}\sigma_2^{\uparrow}\sigma_3^{\downarrow}) & (2.35a) \\ \text{or} \\ 3^{-1/2}(\sigma_1^{\uparrow}\sigma_2^{\downarrow}\sigma_3^{\downarrow} + e^{i2\pi K/3}\sigma_1^{\downarrow}\sigma_2^{\uparrow}\sigma_3^{\downarrow} + e^{i4\pi K/3}\sigma_1^{\downarrow}\sigma_2^{\downarrow}\sigma_3^{\uparrow}) & (2.35b) \end{cases}$$

for which the product $\psi_{JKM}\psi_{\text{nuc}}^{K}$ has the required threefold symmetry. When K is divisible by 3, Eqs. 2.35a and 2.35b reduce to

$$\psi_{\text{nuc}} = \begin{cases} 3^{-1/2}(\sigma_1^{\downarrow}\sigma_2^{\uparrow}\sigma_3^{\uparrow} + \sigma_1^{\uparrow}\sigma_2^{\downarrow}\sigma_3^{\uparrow} + \sigma_1^{\uparrow}\sigma_2^{\uparrow}\sigma_3^{\downarrow}) & (2.36a) \\ \text{or} \\ 3^{-1/2}(\sigma_1^{\uparrow}\sigma_2^{\downarrow}\sigma_3^{\downarrow} + \sigma_1^{\downarrow}\sigma_2^{\uparrow}\sigma_3^{\downarrow} + \sigma_1^{\downarrow}\sigma_2^{\downarrow}\sigma_3^{\uparrow}) & (2.36b) \end{cases}$$

Also,

$$\psi_{\text{nuc}} = \begin{cases} \sigma_1^{\uparrow}\sigma_2^{\uparrow}\sigma_3^{\uparrow} & (2.36c) \\ \text{or} \\ \sigma_1^{\downarrow}\sigma_2^{\downarrow}\sigma_3^{\downarrow} & (2.36d) \end{cases}$$

have the correct symmetry for K divisible by 3. Thus, the statistical weight due to nuclear spin is twice as large for states with K divisible by 3 as for the other states.†

Let us now consider the operation of a 180° rotation about an axis in the plane of the hydrogen nuclei and passing through one of them, equidistant from the other two. This rotation has the same result as the transformation $z_N \rightarrow -z_N$, except that the two off-axis hydrogen nuclei are interchanged. The total wave function must be antisymmetric with respect to the product of these two operations, because the hydrogen nuclei follow Fermi–Dirac statistics. With the nuclei in their equilibrium positions, NH_3 is an oblate symmetric top. Figure 2.1 shows that the energy levels of an asymmetric rotor merge into those of a symmetric top as $\kappa \rightarrow 1$ or -1. The wave functions, however, do not go over into ψ_{JKM} or ψ_{J-KM} when $K \neq 0$, but rather into linear combinations of the form $2^{-1/2}(\psi_{JKM} \pm \psi_{J-KM})$. These are

*If the hydrogen nuclei are numbered 1, 2, and 3, then the permutation 3, 1, and 2 is equivalent to the interchange of 1 with 2 followed by the interchange of 2 with 3.

†To be precise, each of the wave functions in Eqs. 2.35 and 2.36 could be multiplied by one of three possible wave functions for the spin of the ^{14}N nucleus. However, because there is no other nucleus equivalent to the ^{14}N, its spin degeneracy factor has no effect on the spectrum in the approximation that interactions involving spins are neglected.

equally good eigenfunctions for the rigid symmetric top, and are known as Wang symmetric rotor functions. Wave functions antisymmetric to exchange of two hydrogen nuclei can be written as*

$$\psi_{\text{vib-rot-nuc}} = 2^{-1/2}\psi_n(z_N)(\psi_{JKM}\psi^K_{\text{nuc}} \pm \psi_{J-KM}\psi^{-K}_{\text{nuc}}). \tag{2.37}$$

The choice of a plus or minus sign depends on n, J, and K [1, p. 71]; thus, the antisymmetry requirement removes the twofold degeneracy associated with the quantum numbers $\pm K$. However, if $K = 0$, it would be necessary to choose the minus sign when $n + J$ has even parity, and this choice reduces the expression Eq. 2.37 to zero. Hence, alternating energy levels are prohibited; there are *no* microwave inversion lines associated with $K = 0$.

Hyperfine splitting of the NH_3 inversion lines is $\lesssim 2.5$ MHz [28–30]. This splitting can be ignored at the high pressures encountered in the atmospheres of the major planets.

2.3. THERMAL (DOPPLER) BROADENING

Up to this point, the discussion has ignored the translational motion of the molecules. In the absence of collisions, the translational part of the molecular wave function is simply a plane wave, which is separable from the rest of the wave function. The motion of each molecule about its center of mass can then be described as in Section 2.2, except that the line frequencies are Doppler-shifted by a factor proportional to the projection of the molecular velocity along the direction of propagation of the electromagnetic wave. A well-known result of the kinetic theory of gases is that the distribution of velocity components along any fixed direction is Gaussian. Thermally broadened lines, therefore, have the Doppler shape factor,

$$F(\nu, \nu_{fi}) = \pi^{-1/2}\beta_D^{-1}\exp\left[-\left(\frac{\nu - \nu_{fi}}{\beta_D}\right)^2\right] \tag{2.38}$$

where the parameter β_D is given by [64a]

$$\beta_D = \left(\frac{2kT}{mc^2}\right)^{1/2}\nu_{fi} = 4.30 \cdot 10^{-7}\left(\frac{T}{M_m}\right)^{1/2}\nu_{fi} \tag{2.39}$$

in which m is the mass of the molecule, and M_m is its molecular weight in g/mole. The width of the line at half-maximum is $2(\ln 2)^{1/2}\beta_D$. The thermal broadening of typical atmospheric lines is $\sim 10^{-6}$ times the line frequency, and for microwave

*The neglected modes of vibration are assumed to be in their ground states.

lines, it is surpassed by pressure broadening in the stratosphere and troposphere. Section 2.4.2 discusses the case in which both types of broadening are significant.

2.4 PRESSURE BROADENING

2.4.1 General Discussion

Pressure broadening is the perturbation of an absorbing molecule's line spectrum by collisions with other molecules. (The Doppler effect will be ignored until Section 2.4.2.) In a gas of interacting molecules, a potential energy that depends on the relative positions and orientations of the molecules is added to the Hamiltonians for the separate molecules. The result of this alteration to the Hamiltonian is that the gas is able to absorb photons at frequencies well removed from the resonances. In fact, it will be seen that at sufficiently high pressure, even the wings of negative-frequency resonances (which nominally represent emission transitions because $E_f < E_i$) contribute to absorption.

To discuss the effect of collisions, it is helpful to rewrite Eq. 2.1 in a form that emphasizes molecular dynamics. This can be done by introducing the Fourier expansion of the Dirac delta function,

$$\delta(\nu) = \int_{-\infty}^{\infty} e^{i2\pi\nu t}\, dt \tag{2.40}$$

which will enable us to write the absorption spectrum in terms of the Fourier transform of a correlation function. After describing the form of the correlation function in the "impact" approximation, we will obtain the spectrum by taking the transform. Further approximations may be valid in various pressure regimes; Sections 2.4.2 to 2.4.4 consider them in increasing order of pressure.

With the use of Eq. 2.40, and assuming local thermodynamic equilibrium [which implies that $p_a = p_b \exp(-h\nu/kT)$], and also assuming that $h\nu \ll kT$, Eq. 2.1 becomes

$$\alpha(\nu) = \frac{8\pi^3\nu^2}{3ckTV} \int_{-\infty}^{\infty} e^{-i2\pi\nu t}\Phi(t)\, dt \tag{2.41}$$

where $\Phi(t)$ is the correlation function of the total dipole moment $\mathfrak{M}$ in the volume V:

$$\begin{aligned}\Phi(t) &= \sum_{a,b,\sigma} p_b \mathfrak{M}^{\sigma}_{ba} e^{iE_a t/\hbar}\, \mathfrak{M}^{\sigma}_{ab} e^{-iE_b t/\hbar} \\ &= \sum_{a,b,\sigma} p_b \mathfrak{M}^{\sigma}_{ba}(0)\, \mathfrak{M}^{\sigma}_{ab}(t)\end{aligned} \tag{2.42}$$

Each matrix element $\mathfrak{M}^{\sigma}_{ab}(t)$ is equal to an integral similar in form to Eq. 2.11, but with ψ replaced by the time-dependent wave function $\Psi = \psi \exp(-iEt/\hbar)$.

Because $\mathfrak{M}^{\sigma}$ is a Hermitian operator and the statistics of the system are assumed to be stationary, $\Phi(t)$ satisfies the relation

$$\Phi(-t) = \Phi^*(t) \tag{2.43}$$

The product of matrix elements in Eq. 2.42 is weighted by the probability p_b of finding the system in state b, so the sum over all states represents the expected value of the product of matrix elements; hence, a correlation function evaluated for the time delay t. However, Eq. 2.42 is still expressed in terms of states (a, b) of the entire gas within the volume V, whereas we desire a formulation that will yield line shapes associated with transitions between the states of an isolated absorbing molecule. To obtain such a formulation, it is necessary to make some simplifying assumptions concerning collisions.

One very powerful assumption is that of binary collisions: when the density of molecules in the gas is sufficiently low, an absorbing molecule can be considered to interact with one perturbing molecule at a time. Calculations employing the binary-collision approximation have successfully reproduced measured absorption coefficients at pressures as high as 6 atmospheres in NH_3 [31] and 51 atmospheres in O_2 [32]. The first implication of this assumption is that cross-correlations between different absorbing molecules are negligible, so that $\Phi(t)$ can be related to the correlation function $\Phi_1(t)$ for a single absorbing molecule by

$$\Phi(t) = nV\Phi_1(t) \tag{2.44}$$

where n is the number density of the absorbing species. Second, the binary-collision approximation implies that $\Phi_1(t)$ can be evaluated by averaging over all possible collision trajectories, over the distribution of relative speeds between absorbing and perturbing molecules, and over the distribution of initial states of the perturbers.

A further approximation that is widely applied in microwave spectroscopy is the impact approximation, in which $\Phi_1(t)$ is determined by considering only the effects of completed collisions. Hence, it is valid for time intervals $t \gg t_c \simeq 10^{-12}$ s, where t_c is the typical length of time during which molecules interact strongly.

In place of the eigenstates (a, b) of the entire gas, a complete basis in which to represent the Hamiltonian for the two-molecule collision is the product space of states of the isolated molecules. The Hamiltonian can be written as $H_1 + H_2 + \mathcal{V}(t)$, where H_1 and H_2 are Hamiltonians for the isolated absorber and perturber, respectively, and $\mathcal{V}(t)$ is the potential energy of the interaction between the two molecules. This potential is due to the dipole, quadrupole, and higher-order moments of the molecules, whether permanent or induced in the collision [33, Chapter 13; 34].

$\mathcal{V}(t)$ depends on time t through the collision trajectory, which implicitly introduces the "classical-path approximation": that the molecules follow predetermined trajectories (often taken to be straight lines for ease of calculation) instead

of being represented by traveling-wave solutions of the time-dependent Schrödinger equation. From a wave-mechanical viewpoint, the classical path is a geometric-optics approximation, and is therefore valid when the de Broglie wavelength of the perturber is small compared to the size of the intermolecular potential well. At translational energies typical of atmospheric temperatures, this is true for all but the lightest molecules, hydrogen and helium [35]. Furthermore, if the translational motion of the molecules is treated quantum-mechanically [36], the functional form of the line shape is the same as that obtained by use of the classical path.

As a simple example of the effect of collisions on the correlation function, let us consider the system whose energy-level diagram is shown in Figure 2.6. The absorbing molecule has nonzero dipole-moment matrix elements between a lowest state, which is taken as the zero of the energy scale, and several states of higher energy E_f. The dipole-moment matrix elements between states f and f' are zero, but $\mathcal{V}(t)$ has nonzero matrix elements linking these states; thus, the interactions occurring in collisions permit transitions between these states. The transitions due to collisions constitute a Markov random process with constant rates. (A transition rate is the conditional probability per unit time of a transition from one state to another, given that the absorbing molecule is in the former state.) Collisions do not, however, cause interactions involving the lowest state in this example. This is Baranger's [37] "one-state" case. It does not correspond to any situation arising in microwave spectroscopy, but it contains most of the features of the general problem. We consider only positive resonance frequencies for the moment. The dipole-moment correlation function has an exponential form for $t \gg t_c$ [7, 31, 37, 38]:

$$\Phi_1(t) = p_0 \sum_{f,f',\sigma} \mu_{0f}^{\sigma} (e^{i\mathbf{\Omega}t})_{ff'} \mu_{f'0}^{\sigma} \tag{2.45}$$

in which the complex matrix $\mathbf{\Omega}$ has elements

$$\Omega_{ff'} = 2\pi(\delta_{ff'} E_f/h + iR_{ff'}) \tag{2.46}$$

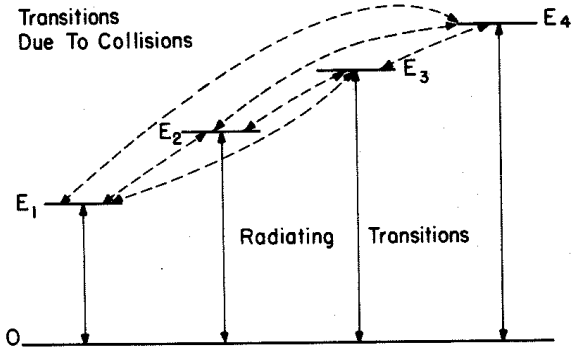

Figure 2.6. The one-state example of pressure broadening.

where $\delta_{ff'}$ is the Kronecker delta. The relaxation matrix $\mathbf{R}$ is calculable from the intermolecular potential [37, 38]. In the binary-collision approximation, $\mathbf{R}$ is proportional to the number density of perturbing molecules. It also depends on temperature through the average over perturber states and speeds. If more than one species of perturber is present in the gas, $\mathbf{R}$ is the sum of contributions from each species.

For $\mathbf{R} = 0$ (no collisions), Eq. 2.45 is a sum of complex exponential functions of time (cosines, if negative resonant frequencies are included) with frequencies E_f/h corresponding to the free motion of the dipole and with amplitudes corresponding to the line intensities. The effect of collisions, expressed by the $\mathbf{R}$ matrix, is to damp out the correlation as $t \to \infty$. This loss of correlation is caused in three ways: a collision can cause a transition to a different energy level, it can temporarily perturb the energy of a state and cause a random change in phase, which is the integral of frequency over time, or it can reorient the rotational motion of the dipole. Collisions of the first type are termed inelastic; the others are elastic collisions. A diagonal element R_{ff} (multiplied by 2π) defines the reciprocal of the mean time interval between "strong" collisions, whether elastic or inelastic, for the state f. An off-diagonal element $2\pi R_{ff'}$ is equal to minus the rate of transitions from f' to f due to inelastic collisions [7]. Both diagonal and off-diagonal elements can be different for different states of the molecule, as can the intermolecular potential.

We now consider the general case in which both upper and lower energy levels of each line are perturbed by collisions and the negative resonant frequencies are included.* To reduce the notational burden, a single index j, which can be positive or negative, will replace in order of frequency the line designation (f, i). A vector $\mathbf{D}$ containing the reduced dipole-moment matrix elements is defined as

$$D_j = \mu_{fi} \tag{2.47a}$$

$$D_{-j} = \mu_{if} \tag{2.47b}$$

In the same vector space, termed the "line space" [37], a diagonal matrix $\mathbf{v}_L$ of line frequencies is defined with

$$(\nu_L)_{jj} = \nu_j = \nu_{fi} \tag{2.48a}$$

$$(\nu_L)_{-j,-j} = \nu_{-j} = \nu_{if} = -\nu_{fi} \tag{2.48b}$$

The diagonal matrix $\mathbf{p}$ of occupation probabilities for microwave lines in local thermodynamic equilibrium has j,jth element

$$p_j = g_i \exp\left[-(E_f + E_i)/2kT\right]/Q(T) \tag{2.49a}$$

*Regarding the negative-frequency resonances, we note that the absorption coefficient $\alpha(\nu)$ must be an even function of ν because a real electromagnetic wave varying as $\cos(2\pi\nu t)$ can be represented by two complex exponentials, $\exp(i2\pi\nu t)$ and $\exp(-i2\pi\nu t)$. If $\alpha(\nu)$ were not even, a real wave would turn into a complex wave as it propagated through the atmosphere.

$$p_{-j} = p_j \tag{2.49b}$$

The correlation function for $t >> t_c$ can then be expressed as [7, 37, 38]

$$\Phi_1(t) = \mathbf{D}^{\mathrm{T}} \exp\,[2\pi t(i\nu_L - \mathbf{R})]\,\mathbf{pD} \tag{2.50}$$

where $\mathbf{R}$ is the relaxation matrix in line space. The elements of $\mathbf{R}$ now contain the influence of perturber interactions with both the upper and lower levels of the lines. As in the one-state case, the correlation function for the free motion of the molecule without collisions ($\mathbf{R} = 0$) is a sum of cosine functions, and $\mathbf{R}$ embodies the effect of the collisions, which damp out the correlation as $t \to \infty$.

To evaluate the Fourier transform in Eq. 2.41 in the impact approximation, one assumes the range of Eq. 2.50 to be $t \geq 0$ and uses Eq. 2.43 and 2.44 to define the correlation function for $t < 0$. The result is [37–39]

$$\alpha(\nu) = \frac{8\pi^2\nu^2 n}{3ckT}\,\mathrm{Im}\,[\mathbf{D}^{\mathrm{T}}(\nu\mathbf{I} - \boldsymbol{\nu}_L - i\mathbf{R})^{-1}\mathbf{pD}] \tag{2.51}$$

where $\mathbf{I}$ is the identity matrix. The matrix $\boldsymbol{\nu}_L + i\mathbf{R}$ can be diagonalized by a transformation of the form $\mathbf{X}^{-1}(\boldsymbol{\nu}_L + i\mathbf{R})\mathbf{X} = \boldsymbol{\Lambda}$ [37, 38]; thus*

$$\alpha(\nu) = \frac{8\pi^2\nu^2 n}{3ckT} \sum_j \frac{\mathrm{Im}\,\Lambda_j\,\mathrm{Re}\,G_{jj} + (\nu - \mathrm{Re}\,\Lambda_j)\mathrm{Im}\,G_{jj}}{(\nu - \mathrm{Re}\,\Lambda_j)^2 + (\mathrm{Im}\,\Lambda_j)^2} \tag{2.52}$$

in which $\mathbf{G} = \mathbf{X}^{-1}\mathbf{pDD}^{\mathrm{T}}\,\mathbf{X}$.

In the binary-collision approximation, the effect of collisions is a modulation of the free dipole motion. Hence the line shape obtained in the impact approximation is valid for frequencies that are displaced from resonance by less than $(2\pi t_c)^{-1} \simeq 100$ GHz. Thus, it can also be used for submillimeter and infrared lines near resonance, but it is not applicable to the microwave tails of those lines. This point will be discussed further in Section 2.4.3 with respect to the spectrum of water vapor.

$\mathbf{X}$, $\boldsymbol{\Lambda}$, and $\mathbf{G}$ depend on the perturber number density (i.e., on pressure) through $\mathbf{R}$. A significant simplification results if we restrict consideration to pressures sufficiently low that only terms up to first order in $\mathbf{R}$ need be retained in $\boldsymbol{\Lambda}$ and $\mathbf{G}$ [40]:

$$\Lambda_j = \nu_j + iR_{jj} + \cdots \tag{2.53}$$

$$G_{jj} = D_j^2 p_j + i2D_j p_j \sum_{j' \neq j} \frac{D_{j'} R_{j'j}}{\nu_j - \nu_{j'}} + \cdots \tag{2.54}$$

*At a given frequency, some of the terms in Eq. 2.52 may be negative because of the $(\nu - \mathrm{Re}\,\Lambda_j)$ factors in their numerators. However, the negative terms will be balanced by corresponding positive contributions in other terms. The overall absorption coefficient for a gas in thermodynamic equilibrium must be positive.

This first-order expansion is applicable for pressures at which the absolute values of the parameters

$$Y_j = \text{Im } G_{jj}/\text{Re } G_{jj} \tag{2.55}$$

are smaller than unity. There is a partial cancellation of higher-order terms [41]. Now, using the line intensity $S_j(T)$ given by Eq. 2.16, we can write Eq. 2.52 as

$$\alpha(\nu) = \frac{n}{\pi} \sum_{j \geq 0} S_j(T) \left(\frac{\nu}{\nu_j}\right)^2 \left[\frac{R_{jj} + (\nu - \nu_j)Y_j}{(\nu - \nu_j)^2 + R_{jj}^2} + \frac{R_{jj} - (\nu + \nu_j)Y_j}{(\nu + \nu_j)^2 + R_{jj}^2}\right] \tag{2.56}$$

The sum in Eq. 2.56 is taken over $j \geq 0$ because negative-frequency resonances are included in the shape factor. If nonresonant absorption ($j = 0$) is present, its line intensity is not defined, but $S_0(T)/\nu_0^2$ has a finite nonzero value as $\nu_0 \to 0$.

For small **R,** Eq. 2.56 approaches the line spectrum of the isolated molecule. The lines have half-widths equal to the diagonal elements of **R.** It has been assumed here that the elements of **R** are purely real. In general, **R** can be complex, although for microwave spectra, the imaginary parts of the elements of **R,** as defined here, are usually much smaller than the real parts. If present, the imaginary parts of the diagonal elements R_{jj} shift the resonant frequencies, as one can see from Eq. 2.53.

The effect of the off-diagonal elements of **R,** which enter Eq. 2.56 through the Y_j, is called line interference, coupling, mixing, blending, or merging. The terms containing Y_j will be significant in Eq. 2.56 only if all of the following conditions are satisfied: (1) At least some of the off-diagonal elements of **R** are comparable in order of magnitude to the diagonal elements. (2) The summation in the imaginary part of Eq. 2.54, in which some of the terms can have opposite sign, does not yield a null result. (3) More than one line contributes significantly to $\alpha(\nu)$.

2.4.2 Low Pressures (Mesosphere and Stratosphere)

If there is no overlap of other lines from the same molecule, including negative-frequency resonances, then the shape factor in Eq. 2.56 can be approximated by the Lorentz shape factor for an isolated line near resonance:

$$F(\nu, \nu_{fi}) = \pi^{-1}(\nu/\nu_{fi})^2 \frac{\gamma_c}{(\nu - \nu_{fi})^2 + \gamma_c^2} \tag{2.57}$$

where $\gamma_c = R_{jj}$ is the collisional half-width for the line. If the line is very narrow compared to its resonant frequency, so that $\nu \approx \nu_{fi}$, then the factor $(\nu/\nu_{fi})^2$ can be omitted. In the stratosphere and mesosphere, pressure broadening is due overwhelmingly to collisions with molecules of the two major constituents, nitrogen and oxygen, which are uniformly mixed. Therefore, the line widths are proportional to the total pressure. From Eqs. 2.12 and 2.57, the absorption coefficient at

the line center is $n_a S_{fi}/\pi\gamma_c$, which is proportional to the mixing ratio of the absorbing gas.

At some pressure level in the mesosphere, the collisional width of a given line decreases to the point that thermal broadening is significant. An assumption that the two broadening processes act independently leads to the Voigt shape factor [42, p. 218]:

$$F(\nu, \nu_{fi}) = \int_{-\infty}^{\infty} F_L(\nu, \nu') F_D(\nu', \nu_{fi})\, d\nu' \tag{2.58}$$

This is the convolution of the Lorentz shape factor F_L given by Eq. 2.57 without the $(\nu/\nu_{fi})^2$ factor, with the Doppler shape factor F_D given by Eq. 2.38. Equation 2.58 neglects the dependence of collisional broadening on the relative speed of the molecules and also neglects the fact that thermal broadening becomes less effective with increasing density* [43, 44; 45, Chapter 7]. However, deviations from the Voigt line shape exceed a few percent only when the perturbing molecule's mass is more than five times the absorber's mass [44, 46].

The half-width at half-maximum of the Voigt function is approximately given by [47]

$$\gamma_V = 0.5346\,\gamma_c + (0.2166\,\gamma_c^2 + 0.6931\,\beta_D^2)^{1/2} \tag{2.59}$$

where β_D is the thermal broadening parameter given by Eq. 2.39. Figure 2.7 plots γ_V versus altitude for two microwave lines of H_2O in the terrestrial atmosphere.

For some purposes, it may be adequate to approximate the combined effect of pressure and thermal broadening by using the collisional line shape, Eq. 2.56 or 2.57, with γ_c replaced by γ_V. However, the collisional shape factors yield higher absorption in the line wings than the Voigt shape factor when $\gamma_c < \beta_D$.

When the detailed shape of a mesospheric line is to be interpreted, the Voigt function can be accurately evaluated by the polynomial expression [48]

$$F(\nu, \nu_{fi}) = \pi^{-1/2}\beta_D^{-1}\,\mathrm{Re}\left[\frac{\sum_{j=0}^{6} a_j \xi^j}{\sum_{j=0}^{7} b_j \xi^j}\right] \tag{2.60}$$

where

$$\xi = \gamma_c/\beta_D + i(\nu - \nu_{fi})/\beta_D \tag{2.61}$$

and the a and b coefficients are listed in Table 2.4. (The imaginary part of this polynomial expression is the dispersion shape factor.)

*The second of these effects is known as collisional narrowing, but actual narrowing of the line would occur only in the absence of pressure broadening (e.g., in nuclear magnetic-resonance spectra).

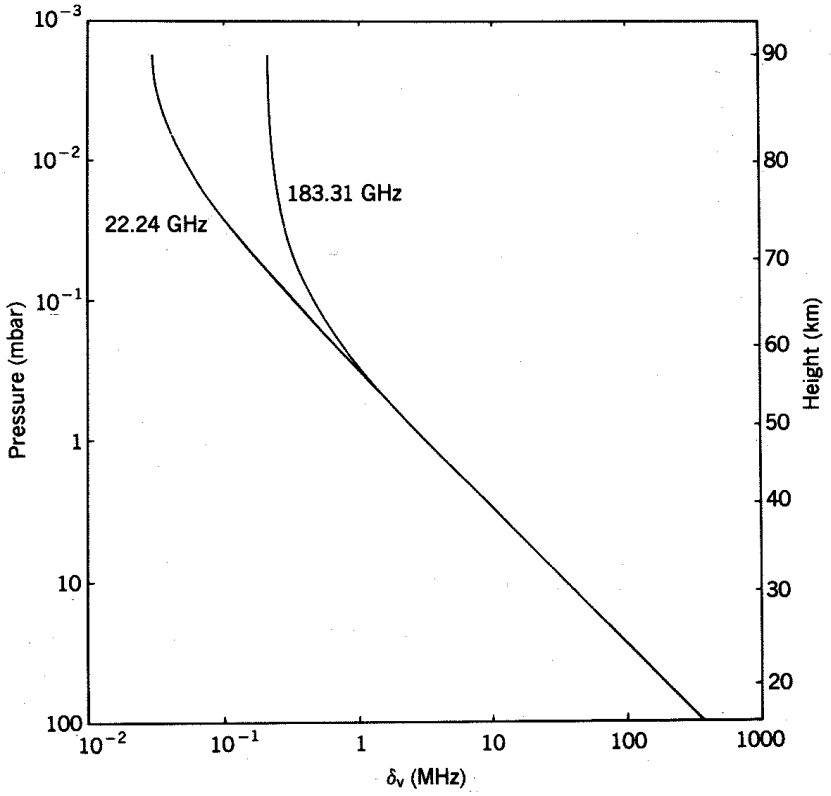

Figure 2.7. Half-widths γ_ν of two H_2O lines in the 1976 U.S. Standard Atmosphere. The transition from predominant thermal broadening to predominant pressure broadening occurs at higher pressure for the higher-frequency line.

Figure 2.8 is an example of a stratospheric oxygen line observed from the ground [49]. Because Zeeman splitting of the line is significant here, the polarization-coherency matrix equation of radiative transfer was used to compute the theoretical curves [24a]. Overlapping oxygen lines in the troposphere attenuate the stratospheric emission (by ~ 6 db), so the full collisional band shape, Eq. 2.56, was used in the calculations. Equation 2.59 was used for the line-width parameter.

TABLE 2.4 Coefficients in Eq. 2.60 for the Voigt Function [48]

j	a_j	b_j
0	122.60793178	122.60793178
1	214.38238869	352.73062511
2	181.92853309	457.33447878
3	93.15558046	348.70391772
4	30.18014220	170.35400182
5	5.91262621	53.99290691
6	0.56418958	10.47985711
7	—	1

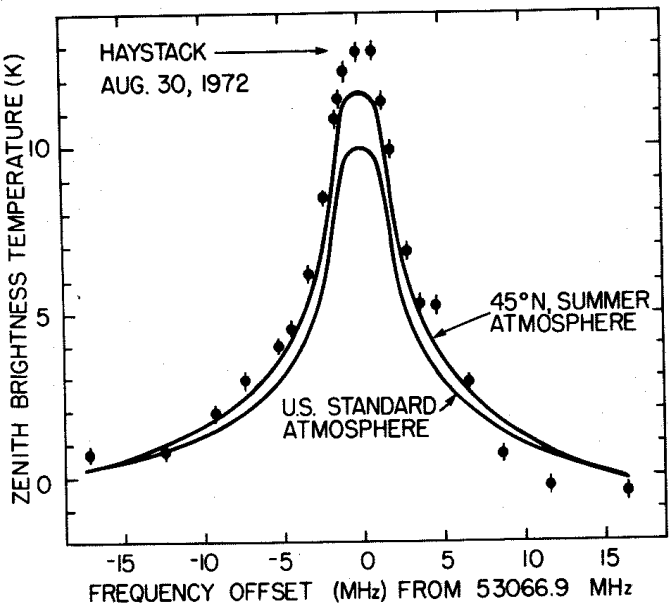

Figure 2.8. Emission from the 27^- line of stratospheric O_2, observed from the ground at Haystack Observatory. The brightness temperature is the average of two orthogonal polarizations, and the scale has an arbitrary zero. Error brackets on the measured points show the rms noise level; the calibration accuracy was estimated to be $\pm 10\%$ [49].

Very little of the emitted energy from this line originates in parts of the atmosphere where thermal broadening predominates; thus, the more precise Voigt function is not required. The curves in Figure 2.8 are calculated for a magnetic field of 0.56 gauss at 18° to the direction of propagation, which was vertical. The two atmospheric models differ by 5 to 10 K at the 30- to 60-km altitudes where the line is formed. This line is very sensitive to stratospheric temperature because of the exponential factor in the line intensity, Eq. 2.16.

2.4.3 Moderate Pressures (Troposphere)

Absorption by tropospheric gases has two consequences for atmospheric remote sensing: it makes possible the sensing of tropospheric temperature and composition, and it attenuates emission from the upper atmosphere when the observer is on the ground. In both respects, tropospheric absorption is dominated by oxygen and water vapor.

At tropospheric pressures, the oxygen lines between roughly 50 and 70 GHz overlap to form an absorption band. Equation 2.56 describes the shape of this band. The nonresonant terms (with $\nu_j = 0$) reduce to the following expression, which has the Debye shape factor:

$$\alpha_0(\nu) = \frac{Cn\gamma_0\nu^2}{T(\nu^2 + \gamma_0^2)} \tag{2.62}$$

where $C = 1.53 \times 10^{-24}$ cm^{2}GHz^{-1}K (theoretical value), and γ_0 is the nonresonant broadening parameter (see Table 2A.1 in the Appendix to Chapter 2). This component contributes a small amount of absorption throughout the microwave spectrum. It accounts for almost all of the absorption by oxygen below 10 GHz, which allows experimental determination of γ_0 [50].

Width parameters for the resonant oxygen lines can be determined from measurements at low pressures, where the line shape near resonance is approximated by Eq. 2.57 [51]. The interference effect, which becomes measurable as the lines begin to overlap, is a linear combination of the Y_j in Eq. 2.56. Measurements at different frequencies reflect different combinations of the Y_j. If the other line parameters are known, determination of the interference parameters is a linear inversion problem [52]; it can be solved by methods similar to those used to infer an atmospheric temperature profile from brightness temperature measurements, given the weighting functions.

Figure 2.9 shows some measurements of absorption and dispersion in the ox-

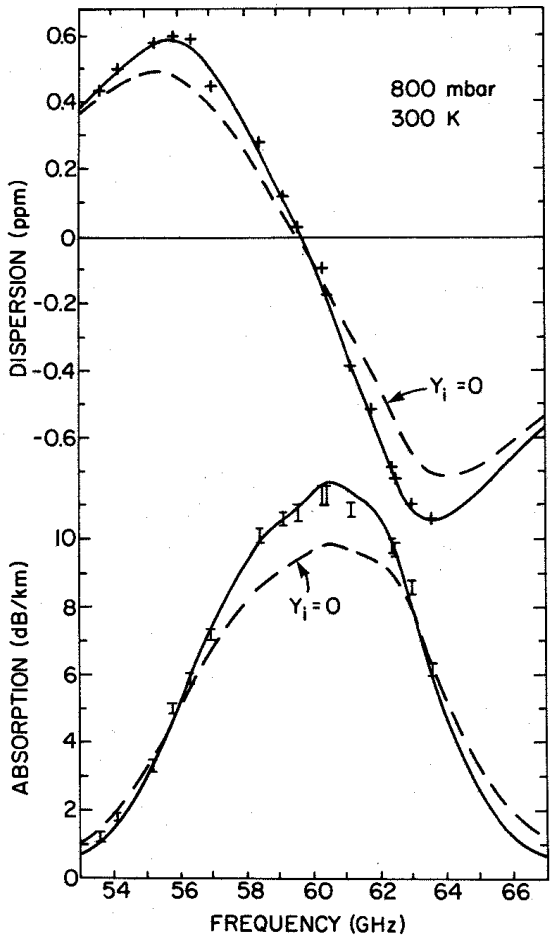

Figure 2.9. Dispersion and absorption in dry air. The difference between the solid and dashed curves is the effect of line coupling in the oxygen band [52].

ygen band [51]. The solid curves are calculated with interference parameters adjusted to fit dispersion, which was measured with greater precision than absorption. Interference parameters on the low side of the band are positive, whereas those on the high side are negative; therefore, the interference effect lowers absorption on the wings and raises it in the middle of the band.

For water vapor, a calculation of the **R** matrix for nine microwave and submillimeter lines yielded off-diagonal elements approximately two orders of magnitude smaller than the diagonal elements [53]. Hence, with $Y \simeq 0$, the frequency dependence of each term in Eq. 2.56 reduces to the shape factor of Van Vleck and Weisskopf [54]:

$$F(\nu, \nu_{fi}) = \pi^{-1}(\nu/\nu_{fi})^2 \left[\frac{\gamma_c}{(\nu - \nu_{fi})^2 + \gamma_c^2} + \frac{\gamma_c}{(\nu + \nu_{fi})^2 + \gamma_c^2} \right] \quad (2.63)$$

Experimental confirmation of Eq. 2.63 has been obtained for the 22-GHz line [55, 56].

However, measurements in both pure water vapor and moist air show more absorption than is contributed by the microwave and submillimeter resonances [55, 57–62]. Along with absorption from the lines listed in the Appendix, it is necessary to add a so-called "continuum" term [62, 63]:

$$\alpha_c(\nu) = (C_s P_{H_2O}^2 \theta^{10.5} + C_f P_{H_2O} P_{dry} \theta^3)\nu^2, \quad (2.64)$$

where $C_s = 1.50 \times 10^{-7}\,\text{cm}^{-1}\text{bar}^{-2}\text{GHz}^{-2}$, $C_f = 4.74 \times 10^{-9}\,\text{cm}^{-1}\text{bar}^{-2}\text{GHz}^{-2}$, $\theta = 300\text{K/T}$, P_{H_2O} is the partial pressure of water vapor, and P_{dry} is the partial pressure of the dry-air components. The coefficients C_s and C_f and the pressure and temperature dependence in Eq. 2.64 were adjusted to fit measurements at 138 GHz, at which frequency the uncertainties in C_s and C_f were estimated as approximately 3% and 1%, respectively [62]. The frequency dependence is based on other measurements [55, 64, 64a].* Of course, the values of these coefficients depend to some extent on the number of lines that are treated as separate contributions and on their assumed shape. The following three paragraphs discuss some of the hypotheses that have been proposed regarding the origin of the absorption represented by Eq. 2.64. (Also see the discussion in Deepak et al. [65a].)

1. *Wings of Infrared Lines* [55]. Because of the microwave region's large displacement in frequency from these resonances, the impact approximation is not valid. However, without using the impact approximation, it is possible to derive an expression having the form of Eq. 2.51 but with **R** depending on ν [66]. Over the microwave spectrum, the frequency dependence of absorption from distant resonances is mostly due to the ν^2 factor in Eq. 2.51. As long as the binary collision approximation is applicable, the pressure dependence of absorption in the

*One set of atmospheric measurements [65] was interpreted as indicating absorption proportional to $P_{H_2O}P_{dry}^2$; however, these measurements can be accounted for by Eq. 2.64 [61].

wings of lines comes from the abundance n of absorbing molecules multiplied by the appropriate elements of **R**, which are proportional to the number density of perturbing molecules. Hence, self-broadening of H_2O produces a $P_{H_2O}^2$ term and foreign-gas broadening produces a $P_{H_2O}P_{dry}$ term. Calculations of pressure broadening for the distant wings of water-vapor lines have been done only with a simplified intermolecular potential, but they yield good agreement with both the magnitude and temperature dependence of Eq. 2.64 [66a].

2. *Collision-induced Absorption* [67, 68]. During close collisions, the intermolecular potential is a large perturbation to the molecular Hamiltonians, and the wave functions are highly distorted in comparison to the isolated molecular wave functions. Hence, the normal selection rules do not hold precisely, and transitions not considered in the previous paragraph may contribute to absorption. This effect has not been calculated rigorously for any molecule of the asymmetric-rotor type.

3. *Water Dimers* [69]. Microwave lines of $(H_2O)_2$ have been detected by molecular-beam techniques [70–71a]. On the basis of these experiments and theoretical calculations, the dimer is believed to have the structure H_2O-HOH, with a hydrogen bond joining the two water molecules. It is a nearly prolate rotor with the energy levels split by several different tunneling motions, giving a complicated microwave spectrum [72]. At atmospheric temperatures several vibrational levels would be excited, and the dimer's molecular parameters are not yet sufficiently well known to calculate its absorption spectrum in the atmosphere. However, numerous overlapping resonances would yield absorption proportional to the dimer abundance, which in thermodynamic equilibrium varies in proportion to the square of the number density of monomers [73]. Hence, it could contribute to the first term in Eq. 2.64. In contradiction to earlier reports of an atmospheric dimer line near 225 GHz [e.g., 73], high-resolution measurements at atmospheric temperatures show no resonant features that can be attributed to dimers [74, 75]. If dimers at atmospheric pressures and temperatures have an unstructured absorption spectrum varying as ν^2, the frequency dependence is accidental.

The common element among these explanations of the water vapor continuum is that the first term in Eq. 2.64 results from the interaction between two water molecules, and the second term is due to the interaction of a water molecule with a nitrogen or oxygen molecule. The explanations differ with regard to the states (bound or free) that are involved in the transitions, and in their wave functions. Thus, the issue is: which states are the most important to consider in a calculation? This is still fertile ground for theorists [76], but for the purpose of calculating atmospheric absorption, one would probably find a parametric approximation such as Eq. 2.64 to be the most convenient model.

Figure 2.10 shows the calculated zenith opacity of the troposphere as a function of frequency for three values of precipitable water content. The water vapor was distributed vertically with constant relative humidity (0%, 17%, 87% for the U.S. Standard Atmosphere). Some measurements corresponding to the highest humidity are plotted by open circles. For the values of H_2O partial pressure in this figure, most of the absorption between lines is due to the second term in Eq. 2.64. Hence,

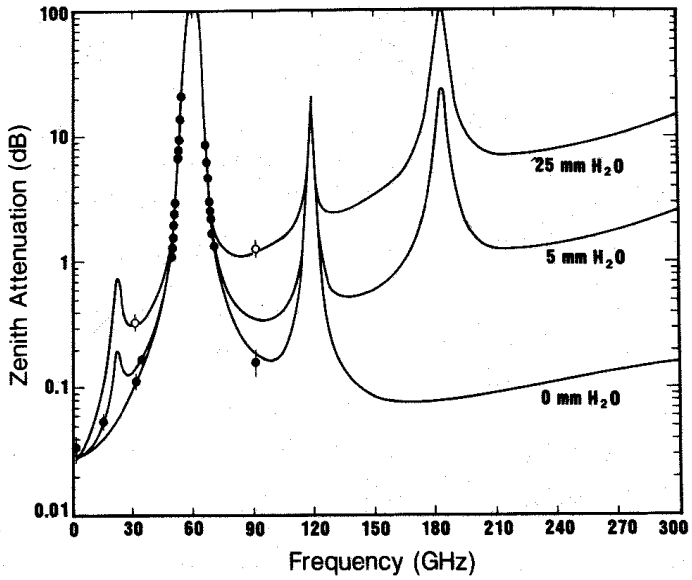

Figure 2.10. Tropospheric (0–11 km) zenith attenuation in the U.S. Standard Atmosphere for three values of precipitable water vapor. Measurements are from References 65 and 75a–75d. The calculated curves include absorption by water vapor, oxygen, and nitrogen. The narrow lines of stratospheric attenuation are not represented here.

the variation of opacity with water vapor is roughly linear; by means of this relation, the opacity for zero water vapor was estimated (filled circles).

At relative humidity $\gtrsim 98\%$, some of the moisture in air is converted to hydrosols (haze, fog or cloud). This source of absorption is outside the subject of this chapter, but is discussed in References 62, 63, 65a, and in Chapter 3.

2.4.4 High Pressures (Deep Planetary Atmospheres)

When pressure broadening causes the lines of a band to overlap so much that structure due to individual resonances is lost, the band can be replaced by one resonance with an average frequency $\bar{\nu}$. If (as for NH_3) there are no other nearby bands and no zero-frequency transitions, line-space vectors then have two elements, corresponding to $-\bar{\nu}$ and $+\bar{\nu}$. Moreover, Ben-Reuven [39] argues that for ammonia, the elements of the relaxation matrix **R** coupling different inversion transitions are much smaller than the diagonal elements.* In this case, **R** reduces to the direct sum of 2×2 matrices (with index values corresponding to $-\nu_{fi}$ and $+\nu_{fi}$) of the form

$$\begin{bmatrix} \gamma_c & -\zeta \\ -\zeta & \gamma_c \end{bmatrix}$$

*The cumulative effect of the former elements at high pressures in pure NH_3 is equivalent to a reduction of γ_c by 6% [77].

for each inversion transition. The off-diagonal elements $-\zeta$ are due to transitions between levels f and i caused by collisions (rather than radiation). By evaluating the matrix inverse in Eq. 2.51, Ben-Reuven obtained the line-shape factor [39, 77]

$$F(\nu, \nu_{fi}) = (2/\pi)(\nu/\nu_{fi})^2 \frac{(\gamma_c - \zeta)\nu^2 + (\gamma_c + \zeta)(\nu_{fi}^2 + \gamma_c^2 - \zeta^2)}{(\nu^2 - \nu_{fi}^2 - \gamma_c^2 + \zeta^2)^2 + 4\nu^2\gamma_c^2} \tag{2.65}$$

This line shape has been used to calculate absorption by NH_3 in the atmosphere of Jupiter [78]. The relationship between Eqs. 2.65 and 2.56 can be seen if ζ^2 is taken to be negligible compared with $\nu_{fi}^2 + \gamma_c^2$. Then $Y = -\zeta/\nu_{fi}$, which is consistent with Eqs. 2.54 and 2.55 in a system having two energy levels.

In the two special cases when $\zeta = 0$ or $\zeta = \gamma_c$, Eq. 2.65 reduces to the shape factors obtained by Van Vleck and Weisskopf [54] and Gross [79], respectively, using classical reasoning. However, the relative sizes of off-diagonal elements of **R** vary with the absorbing and perturbing molecules and are not susceptible to blanket generalizations.

If transitions occur at both zero and nonzero frequencies (as for O_2), **R** can be treated as a 3×3 matrix with indices corresponding to $(-\bar{\nu}, 0, +\bar{\nu})$ at high pressures or when the observed frequency is far from the resonant band [80, 81].

When a band of merged lines is considered as a single resonance, the ratio γ_c/P is typically smaller than for the individual lines when they are resolved at lower pressures [80, 81]. For example, if in Figure 2.6 the energies $E_1, \cdots, E_4$ were equal, to within the width of the lines, then collisions would reduce the correlation function by virtue of their effect on the phase or spatial orientation of the radiation, but not by transfers from one state to another. This effect can be seen in Figure 2.9, where line interference acts to make the resonance narrower than would be predicted by consideration only of the diagonal elements of **R.**

At gas densities so high that γ_c approaches $(2\pi t_c)^{-1} \simeq 100$ GHz, both the impact approximation and the binary-collision approximation are no longer valid, and the relaxation matrix is not simply proportional to density. Theoretical investigations are more difficult in this pressure regime, but at least in principle, the problem can be approached through use of techniques such as cumulant expansions [82].

2.5 COLLISION-INDUCED ABSORPTION BY NITROGEN AND CARBON DIOXIDE

N_2 and CO_2 have no permanent dipole moments, and, therefore, isolated molecules of these gases do not exhibit pure rotational spectra. (CO_2 does have an infrared vibration–rotation spectrum.) However, these molecules possess electric quadrupole moments, and during collisions, the quadrupole moment of one molecule interacts with the polarizability of its partner to induce a dipole moment in the partner molecule. The matrix elements of an induced dipole do not follow the

selection rules applicable to a dipole moment fixed in the molecule. The selection rules for an induced dipole are those of the inducing multipole moment [83]; in the case of a quadrupole, $|\Delta J| = 0$ or 2.

The correlation function for the induced dipole consists of a short pulse, whose length is determined by the collision duration, modulating the transition frequency. The width of a collision-induced resonance (which is the Fourier transform of the correlation function) is, therefore, on the order of 300 to 1000 GHz or more, and it is independent of the gas density. In the microwave part of the spectrum, the frequency dependence of absorption comes from the ν^2 factor in Eq. 2.41.

The number of binary collisions per unit time in a given volume is one-half the number of molecules divided by the mean time between collisions for each molecule. This mean time varies inversely with number density n, so collision-induced absorption varies as n^2 for identical molecules or $n_1 n_2$ for unlike molecules.

In a mixture of N_2 and CO_2, collision-induced absorption can be calculated by the empirical expression [84, 85]

$$\alpha(\nu) = (C_{N_2} P_{N_2}^2 \theta^{3.55} + C_{N_2-CO_2} P_{N_2} P_{CO_2} \theta^{4.7} + C_{CO_2} P_{CO_2}^2 \theta^{5.08}) \nu^2 \quad (2.66)$$

where

$$C_{N_2} = 1.05 \times 10^{-12} \text{ cm}^{-1}\text{bar}^{-2}\text{GHz}^{-2} \quad [85]$$

$$C_{N_2-CO_2} = 2.71 \times 10^{-11} \text{ cm}^{-1}\text{bar}^{-2}\text{GHz}^{-2} \quad [84]$$

$$C_{CO_2} = 7.43 \times 10^{-11} \text{ cm}^{-1}\text{bar}^{-2}\text{GHz}^{-2} \quad [85]$$

$\theta = 300/T$, and P_{N_2} and P_{CO_2} are the partial pressures of the two gases. The ideal-gas law has been used here to substitute pressure for density.

In the terrestrial atmosphere, the second and third terms in Eq. 2.66 are negligible. The first term contributes a small amount of absorption that may be noticeable in a dry atmosphere for $\nu \gtrsim 150$ GHz. It is responsible for the high-frequency upturn of the 0-mm H_2O curve in Figure 2.10. One could add a contribution from induced absorption in N_2-O_2 collisions, but this would be a minor correction.

In the atmosphere of Venus, CO_2 is a major contributor to microwave opacity. Equation 2.66 is probably accurate to $\sim 20\%$ for conditions on Venus. It can be improved by corrections for departures from the ideal-gas law and from the ν^2 dependence at high frequencies, and by corrections for three-body collisions [85, 86].

Acknowledgments

The author thanks P. G. Bonanni, A. J. Gasiewski, J. Langen, D. H. Staelin, M. W. P. Strandberg, and S. Walter for their comments on the manuscript.

REFERENCES

1. C. H. Townes and A. L. Schawlow, *Microwave Spectroscopy*. McGraw-Hill, New York, 1955.
2. W. Gordy, W. V. Smith, and R. F. Trambarulo, *Microwave Spectroscopy*. Dover, New York, 1966.
3. W. Gordy and R. L. Cook, *Microwave Molecular Spectra*. Wiley, New York, 1984.
4. M. W. P. Strandberg, *Microwave Spectroscopy*. Wiley, New York, 1954.
5. G. Herzberg, *Spectra of Diatomic Molecules*. Van Nostrand-Reinhold, New York, 1950.
6. G. Herzberg, *Infrared and Raman Spectra of Polyatomic Molecules*. Van Nostrand-Reinhold, New York, 1945.
7. R. G. Gordon, Correlation functions for molecular motion. *Adv. Magn. Reson.* **3,** 1–42 (1968).
8. J. H. R. Clarke, Band shapes and molecular dynamics in liquids. *Adv. Infrared Raman Spectrosc.* **4,** 109–193 (1978).
9. L. Pauling and E. B. Wilson, *Introduction to Quantum Mechanics*. McGraw-Hill, New York, 1935.
10. A. R. Edmonds, *Angular Momentum in Quantum Mechanics*. Princeton University, Princeton, New Jersey, 1974.
11. G. W. King, R. M. Hainer, and P. C. Cross, The asymmetric rotor. 1. Calculation and symmetry classification of energy levels. *J. Chem. Phys.* **11,** 27–40 (1943).
12. F. C. DeLucia, P. Helminger, R. L. Cook, and W. Gordy, Submillimeter microwave spectrum of $H_2{}^{16}O$. *Phys. Rev. A* **5,** 487–490 (1972).
13. R. K. Kakar, E. A. Cohen, and M. Geller, The rotational spectrum and molecular parameters of ClO in the $v = 0$ and $v = 1$ states. *J. Mol. Spectrosc.* **70,** 243–256 (1978).
14. T. Amano, S. Saito, E. Hirota, Y. Morino, D. R. Johnson, and F. X. Powell, Microwave spectrum of the ClO radical. *J. Mol. Spectrosc.* **30,** 275–289 (1969).
15. T. T. Wilheit and A. H. Barrett, Microwave spectrum of molecular oxygen. *Phys. Rev. A* **1,** 213–215 (1970).
16. N. Basco and R. D. Morse, The vacuum ultraviolet absorption spectrum of ClO. *J. Mol. Spectrosc.* **45,** 35–45 (1973).

16a. J. M. Moran et al., Very long baseline interferometric observations of the H_2O sources in W49N, W3(OH), Orion A, and VY Canis Majoris. *Astrophys. J.* **185,** 535–567 (1973); see Fig. 14.

17. H. M. Pickett, D. E. Brinza, and E. A. Cohen, Pressure broadening of ClO by nitrogen. *J. Geophys. Res.* **86,** 7279–7282 (1981).
18. A. Carrington, P. N. Dyer, and D. H. Levy, Gas-phase electron resonance spectrum of ClO. *J. Chem. Phys.* **47,** 1756–1763 (1967).
19. J. H. Van Vleck, The absorption of microwaves by oxygen. *Phys. Rev.* **71,** 413–424 (1947).
20. M. Tinkham and M. W. P. Strandberg, Theory of the fine structure of the molecular oxygen ground state. *Phys. Rev.* **97,** 937–951 (1955).

21. M. Tinkham and M. W. P. Strandberg, Interaction of molecular oxygen with a magnetic field. *Phys. Rev.* **97,** 951–966 (1955).

22. J. H. Van Vleck, Magnetic dipole radiation and the atmospheric absorption bands of oxygen. *Astrophys. J.* **80,** 161–170 (1934).

23. H. J. Liebe, Modeling attenuation and phase of radio waves in air at frequencies below 1000 GHz. *Radio Sci.* **16,** 1183–1199 (1981).

24. W. B. Lenoir, Microwave spectrum of molecular oxygen in the mesosphere. *J. Geophys. Res.* **73,** 361–376 (1968).

24a. P. W. Rosenkranz and D. H. Staelin, Polarized thermal microwave emission from oxygen in the mesosphere. *Radio Sci.* **23,** 721–729 (1988).

25. W. B. Lenoir, Propagation of partially polarized waves in a slightly anisotropic medium. *J. Appl. Phys.* **38,** 5283–5290 (1967).

26. R. L. Poynter and R. K. Kakar, The microwave frequencies, line parameters, and spectral constants for $^{14}NH_3$. *Astrophys. J. Suppl. no. 277,* **29,** 87–96 (1975).

27. N. Husson, A. Goldman, and G. Orton, Spectroscopic line parameters of NH_3 and PH_3 in the far infrared. *J. Quant. Spectrosc. Radiat. Transfer* **27,** 505–515 (1982).

28. G. R. Gunther-Mohr, R. L. White, A. L. Schawlow, W. E. Good, and D. K. Coles, Hyperfine structure in the spectrum of $N^{14}H_3$. I. Experimental results. *Phys. Rev.* **94,** 1184–1191 (1954).

29. G. R. Gunther-Mohr, C. H. Townes, and J. H. Van Vleck, Hyperfine structure in the spectrum of $N^{14}H_3$. II. Theoretical discussion. *Phys. Rev.* **94,** 1191–1203 (1954).

30. S. G. Kukolich, Measurement of ammonia hyperfine structure with a two-cavity maser. *Phys. Rev.* **156,** 83–92 (1967).

31. J. I. Gersten and H. M. Foley, Theory of pressure broadening of microwave spectral lines. *Phys. Rev.* **182,** 24–38 (1969).

32. U. Mingelgrin and R. G. Gordon, The interaction potential and the determination of some cross sections and spectra of pure O_2 and O_2-Ar gas mixtures. *J. Chem. Phys.* **70,** 3828–3839 (1979).

33. J. O. Hirschfelder, C. F. Curtiss, and R. B. Bird, *Molecular Theory of Gases and Liquids*. Wiley, New York, 1954.

34. G. Birnbaum, Microwave pressure broadening and its application to intermolecular forces. *Adv. Chem. Phys.* **12,** 487–548 (1967).

35. P. W. Anderson, Pressure broadening in the microwave and infra-red regions. *Phys. Rev.* **76,** 647–661 (1949).

36. M. Baranger, General impact theory of pressure broadening. *Phys. Rev.* **112,** 855–865 (1958).

37. M. Baranger, Problem of overlapping lines in the theory of pressure broadening. *Phys. Rev.* **111,** 494–504 (1958).

38. A. C. Kolb and H. Griem, Theory of line broadening in multiplet spectra. *Phys. Rev.* **111,** 514–521 (1958).

39. A. Ben-Reuven, Impact broadening of microwave spectra. *Phys. Rev.* **145,** 7–22 (1966).

40. P. W. Rosenkranz, Shape of the 5-mm oxygen band in the atmosphere. *IEEE Trans. Antennas Propag.* **AP-23,** 498–506 (1975).

41. E. W. Smith, Absorption and dispersion in the O_2 microwave spectrum at atmospheric pressures. *J. Chem. Phys.* **74,** 6658–6673 (1981).

42. B. H. Armstrong and R. W. Nicholls, *Emission, Absorption and Transfer of Radiation in Heated Atmospheres*. Pergamon, Oxford, 1972.

43. J. I. Gersten and H. M. Foley, Combined Doppler and collision broadening. *J. Opt. Soc. Am.* **58,** 933–937 (1968).

44. J. Ward, J. Cooper, and E. W. Smith, Correlation effects in the theory of combined Doppler and pressure broadening. I. Classical theory. *J. Quant. Spectrosc. Radiat. Transfer* **14,**555–590 (1974).

45. R. G. Breene, Jr., *Theories of Spectral Line Shape*. Wiley, New York, 1981.

46. D. G. McCartan and N. Lwin, Correlations between Doppler and collision broadening in neutral-atom line broadening. *J. Phys. B* **10,** L17–L20 (1977).

47. J. J. Olivero and R. L. Longbothum, Empirical fits to the Voigt line width: A brief review. *J. Quant. Spectrosc. Radiat. Transfer* **17,** 233–236 (1977).

48. A. K. Hui, B. H. Armstrong, and A. A. Wray, Rapid computation of the Voigt and complex error functions. *J. Quant. Spectrosc. Radiat. Transfer* **19,** 509–516 (1978).

49. J. W. Waters, Ground-based measurement of millimetre-wavelength emission by upper stratospheric O_2. *Nature (London)* **242,** 506–508 (1973).

50. A. A. Maryott and G. Birnbaum, Microwave absorption in compressed oxygen. *J. Chem. Phys.* **32,** 686–691 (1960).

51. H. J. Liebe, G. G. Gimmestad, and J. D. Hopponen, Atmospheric oxygen microwave spectrum—experiment versus theory. *IEEE Trans. Antennas Propag.* **AP-25,** 327–335 (1977).

52. P. W. Rosenkranz, Interference coefficients for overlapping oxygen lines in air. *J. Quant. Spectrosc. Radiat. Transfer* **39,** 287–297 (1988).

53. K. S. Lam, Application of pressure broadening theory to the calculation of atmospheric oxygen and water vapor microwave absorption. *J. Quant. Spectrosc. Radiat. Transfer* **17,** 351–383 (1977).

54. J. H. Van Vleck and V. F. Weisskopf, On the shape of collision-broadened lines. *Rev. Mod. Phys.* **17,** 227–236 (1945).

55. G. E. Becker and S. H. Autler, Water vapor absorption of electromagnetic radiation in the centimeter wave-length range. *Phys. Rev.* **70,** 300–307 (1946).

56. R. J. Hill, Water vapor absorption line shape comparison using the 22-GHz line: The Van Vleck-Weisskopf shape affirmed. *Radio Sci.* **21,** 447–451 (1986).

57. T. Manabe, R. O. Debolt, and H. J. Liebe, Moist-air attenuation at 96 GHz over a 21-km line-of-sight path. *IEEE Trans. Antennas Propag.* **AP-37,** 262–266 (1989).

58. L. Frenkel and D. Woods, The microwave absorption by H_2O vapor and its mixtures with other gases between 100 and 300 Gc/s. *Proc. IEEE* **54,** 498–505 (1966).

59. D. E. Burch, Continuum absorption by atmospheric H_2O. *Proc. SPIE—Int. Soc. Opt. Eng.* **277,** 28–39 (1981).

60. H. J. Liebe, The atmospheric water vapor continuum below 300 GHz. *Int. J. Infrared Millimeter Waves* **5,** 207–227 (1984).

61. H. J. Liebe, An updated model for millimeter wave propagation in moist air. *Radio Sci.* **20,** 1069–1089 (1985).

62. H. J. Liebe, A contribution to modeling atmospheric millimeter-wave properties. *Frequenz* **41,** 31–36 (1987).

63. H. J. Liebe, MPM—An atmospheric millimeter-wave propagation model. *Int. J. Infrared Millimeter Waves* **10,** 631–650 (1989).

64. N. E. Gaut and E. C. Reifenstein, III, *Environ. Res. Tech. Rep.* **13** (1971), quoted in Waters [64a].

64a. J. W. Waters, Absorption and emission by atmospheric gases. *Methods of Experimental Physics vol. 12B*, pp. 142–176 (M. L. Meeks, ed.) Academic Press, New York, 1976.

65. D. C. Hogg, F. O. Guiraud, and E. R. Westwater, Emission measurements of 31.6 GHz absorption by atmospheric water vapor. *Radio Sci.* **18,** 1295–1300 (1983).

65a. A. Deepak, T. D. Wilkerson, and L. H. Ruhnke, eds., *Atmospheric Water Vapor.* Academic Press, New York, 1980.

66. U. Fano, Pressure broadening as a prototype of relaxation. *Phys. Rev.* **131,** 259–268 (1963).

66a. Q. Ma and R. H. Tipping, Water vapor continuum in the millimeter spectral region. *J. Chem. Phys.* **93,** 6127–6139 (1990).

67. A. A. Maryott and G. Birnbaum, Line shape and collision effects in the microwave wing of far-infrared rotational lines. *J. Chem. Phys.* **47,** 3200–3205 (1967).

68. L. Frenkel, The influence of molecular multipole moments on the dielectric relaxation of polar gases. *J. Mol. Spectrosc.* **26,** 227–236 (1968).

69. A. A. Viktorova and S. A. Zhevakin, Absorption of microwaves in air by water-vapor dimers. *Sov. Phys.—Dokl. (Engl. Transl.)* **11,** 1065–1068 (1967); *Dokl. Akad. Nauk SSSR* **171,** 1061–1064 (1966).

70. T. R. Dyke, K. M. Mack, and J. S. Muenter, The structure of water dimer from molecular beam electric resonance spectroscopy. *J. Chem. Phys.* **66,** 498–510 (1977).

71. L. H. Coudert, F. J. Lovas, R. D. Suenram, and J. T. Hougen, New measurements of microwave transitions in the water dimer. *J. Chem. Phys.* **87,** 6290–6299 (1987).

71a. J. A. Odutola, T. A. Hu, D. Prinslow, S. E. O'Dell, and T. R. Dyke, Water dimer tunneling states with K = 0. *J. Chem. Phys.* **88,** 5352–5361 (1988).

72. T. R. Dyke, Group theoretical classification of the tunneling-rotational energy levels of water dimer. *J. Chem. Phys.* **66,** 492–497 (1977).

73. H. A. Gebbie, W. J. Burroughs, J. Chamberlin, J. E. Harries, and R. G. Jones, Dimers of the water molecule in the Earth's atmosphere. *Nature (London)* **221,** 143–145 (1969).

74. D. P. Rice and P. A. R. Ade, Absolute measurements of the atmospheric transparency at short millimetre wavelengths. *Infrared Phys.* **19,** 575–584 (1979).

75. A. J. Kemp, J. R. Birch, and M. N. Afsar, The refractive index of water vapour: A comparison of measurement and theory. *Infrared Phys.* **18,** 827–833 (1978).

75a. T. F. Howell and J. R. Shakeshaft, Attenuation of radio waves by the troposphere over the frequency range 0.4–10 GHz. *J. Atmos. Terr. Phys.* **29,** 1559–1571 (1967).

75b. E. E. Altshuler, V. J. Falcone, Jr., and K. N. Wulfsberg, Atmospheric effects on propagation at millimeter wavelengths. *IEEE Spectrum* **5**(7), 83–90 (1968).

75c. E. E. Reber, Absorption of the 4- to 6-millimeter wavelength band in the atmosphere. *J. Geophys. Res.* **77,** 3831–3845 (1972).

75d. F. I. Shimabukuro and E. E. Epstein, Attenuation and emission of the atmosphere at 3.3 mm. *IEEE Trans. Antennas Propag.* **AP-18,** 485–490 (1970).

76. E. Hudis, Y. Ben-Aryeh, and U. P. Oppenheim, The contribution of third order linear

absorption to the water vapor continuum. *J. Quant. Spectrosc. Radiat. Transfer* **47**, 319–323, (1992).

77. A. Ben-Reuven, Transition from resonant to nonresonant line shape in microwave absorption. *Phys. Rev. Lett.* **14,** 349–351 (1965).
78. G. T. Wrixon, W. J. Welch, and D. D. Thornton, The spectrum of Jupiter at millimeter wavelengths. *Astrophys. J.* **169,** 171–183 (1971).
79. E. P. Gross, Shape of collision-broadened spectral lines. *Phys. Rev.* **97,** 395–403 (1955).
80. R. G. Gordon, On the pressure broadening of molecular multiplet spectra. *J. Chem. Phys.* **46,** 448–455 (1967).
81. A. Ben-Reuven and A. Lightman, Impact broadening of the oxygen microwave spectrum. *J. Chem. Phys.* **46,** 2429–2430 (1967).
82. A. Royer, Shift, width, and asymmetry of pressure-broadened spectral lines at intermediate densities. *Phys. Rev. A* **22,** 1625–1654 (1980).
83. G. Birnbaum, B. Guillot, and S. Bratos, Theory of collision-induced line shapes—absorption and light scattering at low density. *Adv. Chem. Phys.* **51,** 49–112 (1982).
84. W. Ho, I. A. Kaufman, and P. Thaddeus, Laboratory measurement of microwave absorption in models of the atmosphere of Venus. *J. Geophys. Res.* **71,** 5091–5108 (1966).
85. I. R. Dagg, G. E. Reesor, and J. L. Urbaniak, Collision induced absorption in N_2, CO_2, and H_2 at 2.3 cm^{-1}. *Can. J. Phys.* **53,** 1764–1776 (1975).
86. I. R. Dagg, G. E. Reesor, and M. Wong, A microwave cavity measurement of collision-induced absorption in N_2 and CO_2 at 4.6 cm^{-1}. *Can. J. Phys.* **56,** 1037–1045 (1978).